The Pennsylvania State University

The Graduate School

College of Earth and Mineral Sciences

ABRUPT CHANGES IN ICE SHELVES AND ICE STREAMS: MODEL STUDIES

A Thesis in

Geosciences

by

Todd K. Dupont

Submitted in Partial Fulfillment
of the Requirements
for the Degree of

Doctor of Philosophy

May 2004

The thesis of Todd K. Dupont has been reviewed and approved* by the following:

Richard B. Alley
Evan Pugh Professor of Geosciences
Thesis Advisor
Chair of Committee

Derek Elsworth
Professor of Energy and Geo-Environmental Engineering

James F. Kasting
Distinguished Professor of Geosciences

Raymond G. Najjar
Associate Professor of Meteorology & Geosciences

Peter Deines
Professor of Geochemistry
Associate Head for Graduate Programs and Research

*Signatures are on file in the Graduate School.

Abstract

Ice sheets are among the most important components of the Earth system because of their ability to force changes in climate and sea level. Ice streams are efficient pathways of mass flux from the interior of ice sheets. Thus an understanding of ice-stream dynamics is integral to an understanding of ice sheets and their interplay with sea level and climate.

Here a 1-d model of the coupled mass and momentum balance of ice streams and shelves is developed. Longitudinal deviatoric stress is included in the force-balance component model. The mass-balance component model is time-dependent and thus allows simulation of the dynamic consequences of changes in boundary conditions or parameters. An improved, computationally efficient algorithm of the discretization of the mass-balance equation is outlined. All model parameters are non-dimensional.

The model is applied to two problems. In the first study we address the sensitivity of ice-stream/ice-shelf systems to changes in ice-shelf buttressing. We find that for reasonable parameter values such systems are markedly sensitive to a loss of buttressing. Response includes net grounding-line retreat on the order of 10% of the length scale for the system and a roughly 30% loss in the volume of ice above flotation. In the second study we examine the conditions under which ice flowing over a sill will tend to create a reversed ice/air surface slope. Here we find that such slope reversals occur within the range of reasonable parameter values, and thus should be expected. Hence, ice shelf grounding on a sill can trap water and drive subsequent thickening, eventually tending toward outburst flooding.

Table of Contents

List of Tables

List of Figures

Acknowledgments

This work was funded by various NSF grants including Nos. 9870886, 0126187, 9614927, 9526374, and 9417848.

I gratefully acknowledge the love and support provided by my family: Judy Dupont, Todd F. Dupont, my sister Michelle D. Brown, and her clan. They have my particular gratitude for their forgiveness and forbearance through my many youthful moods, mistakes and offenses.

There many mentors, advisors and colleagues to thank. Douglas MacAyeal has helped me in numerous ways through the years, starting when I was an rudderless undergraduate. If it weren't for his guidance and example over the years, I doubt that I would have become an ice modeler. Byron and Heather Parizek have been good friends and sage advisors ever since my arrival at Penn State in 1996, brightening my spirits with their humor and kindness. Kirk Maasch, Terry Hughes and James Fastook, all at U. Maine, helped shape me into a quantitative earth scientist, and provided me with vivid proof that theory needn't be devoid of personality. Marjorie Schmeltz and Eric Rignot, of JPL, jumpstarted my interest in Pine Island Glacier. The help and advice of Dr. Ryan Elmore, a former house-mate, fellow grad student, and resident statistical and linux guru, saved my bacon many times. I also thank the present and former members of the Ice and Climate Research group here at Penn State, including Matt Spencer, Sarah Das, Tim Creyts, David B. Reusch, Anna María Ágústsdóttir Sridhar Anandakrishnan, Don Voigt, David Pollard, and those of a more recent vintage.

I deeply appreciate the commitment, patience, and insightful advice of my doctoral committee, Drs. Richard B. Alley, Derek Elsworth, James Kasting and Raymond Najjar, which has been of immeasurable aid.

Having Richard B. Alley as my doctoral advisor has been an absolutely amazing experience. He has gone above and beyond the call of duty many times and on many fronts, including his always-open door, beating many fast-approaching NSF-proposal deadlines, sending his theoretical glaciology students to Siple Dome, having us attend overseas conferences, and prodding with his infamous "progress???" emails. It has been a privilege to be a Richard B. Alley student, and I thank him for his invaluable advice, support, and friendship.

Preface

This dissertation is dedicated in loving memory of my Grandmother,

Roberta Alexander

(1916-2003)

She had a wonderful sense of humor, an inquisitive mind, and she was an unwaivering supporter of education and the scientific endeavor. I miss her very much.

Chapter 1

Introduction

Ice sheets are agents of sea-level, climate and geomorphological dynamics. Ice sheets are reservoirs of water and thus sea level: if the present-day Greenland and Antarctic ice sheets were to melt, sea level would rise approximately 75 meters [*Warrick et al.*, 1995, p. 372]. During the last glacial maximum ($\sim$ 25 ka) sea level was approximately 120 meters lower than present, suggesting that ice sheets held $\sim$200 meters of sea-level equivalent at that time. Thus, the mass balance of ice sheets plays a key part in the evolution of sea level. Through feedbacks with the atmosphere and ocean, ice sheets also influence climate dynamics. One of these is the ice/albedo feedback, which taken to its extreme runs away to the hypothesized snowball-earth [e.g., *Hoffman et al.*, 1998]. Climate also feels the effects of ice sheets through the influence of injections of ice-berg armadas and meltwater pulses on ocean circulation [e.g., *Broecker*, 1994; *Bond et al.*, 1999]. The geomorphic power of ice sheets and glaciers is evidenced in vast till sheets [*Alley*, 1991] and overdeepenings [*Alley et al.*, 2003b].

1.1 Sea level, marine-ice-sheet instability and buttressing

In 1968, Mercer called into question the stability of the West Antarctic Ice Sheet (WAIS, see figure 1.1) on the basis of geologic evidence for a sea-level high-stand during the previous interglacial ($\sim$120 ka) that was approximately 5 meters higher than present

[*Mercer*, 1968]. The suggestion was that the WAIS, which presently holds the equivalent of $\sim$ 5.5 meters of sea level ([e.g., *Drewry*, 1983]), has collapsed relatively recently in geologic terms. *Scherer et al.* [1998] used diatom and ^{10}Be evidence to confirm the notion of recent WAIS collapse, albeit only pinning the timing of this collapse to the late Pleistocene. The implication of a recent WAIS collapse is that if this ice sheet has a natural tendency toward collapse, then it is plausible that this ice sheet will collapse again, either naturally or in response to anthropogenic forcing.

The work of *Weertman* [1961, 1974] and *Thomas and Bentley* [1978] bolstered this notion of WAIS collapse by identifying and simulating a physically plausible mechanism for such a collapse. The main idea is that a marine ice sheet (one whose bed is generally well below sea-level), such as the WAIS, is fundamentally unstable due to a positive feedback between the flux and thickness at the grounding line, where ice from the interior goes afloat as it flows into the surrounding ice shelves. Clearly then, the viability of this "marine-ice-sheet instability" mechanism hinges on correctly modeling the nature of the feedback between grounding-line thickness and flux. This flux is dominated by ice streams, which drain the interior of the ice sheet. Therefore, the crux of the instability lies in resolving the physical interaction between ice streams and ice shelves.

The stress condition at the grounding line is one facet of this interaction. Of particular import is the concept of ice-shelf buttressing, wherein the ice shelf buffers the grounded ice from the stretching force that would apply if the ice front were at the grounding line. The stretching force derives from the difference between the depth-integrated static pressures within the ice and the ocean, respectively. The stretching force yields a positive depth-integrated longitudinal (along-flow) deviatoric stress. Figure (1.2)

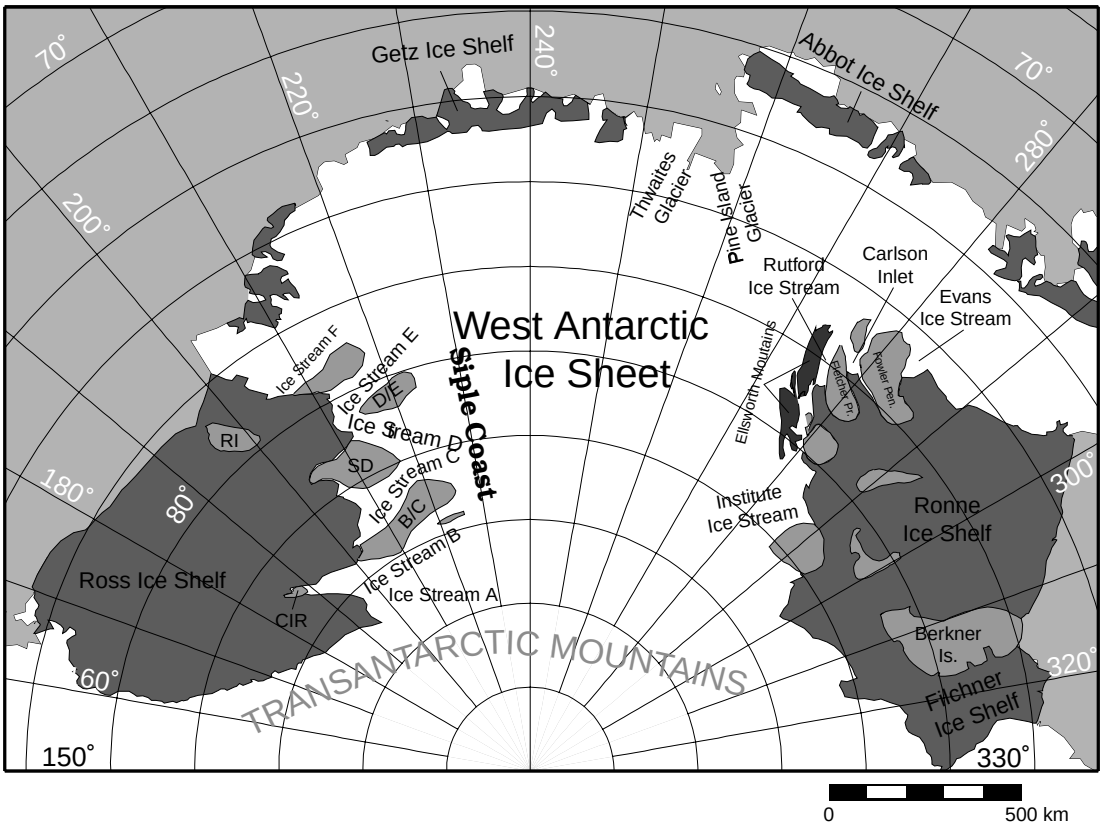

Fig. 1.1. Location map for the West Antarctic Ice Sheet, modified from *Alley and Bindschadler* [2001].

shows the origin of this stretching force at an ice front, the map-view boundary between the ice shelf and the ocean. Buttressing reduces the stretching force required, and is accomplished by the ice shelf through drag along its lateral boundaries and through drag in localized areas of grounding.

Van der Veen [1986] attempted to model the interplay between grounded and floating (shelf) ice by specifying a transition zone for the stress regime, going from the longitudinal-deviatoric-dominated regime near the grounding line to what is presumed to be the vertical-shear-dominated regime upglacier. *Van der Veen* [1986] assumed that in this transition zone the longitudinal deviatoric stress decays linearly to zero as one moves upglacier. In addition, he derived the longitudinal deviatoric stress applied at the grounding line from the assumption of an appended ice shelf at equilibrium. The main advantage of this model was that it was simple to implement within the context of coarser-resolution models of inland ice flow. Unfortunately, the ad-hoc treatment of the longitudinal deviatoric stress and the assumption of equilibrium ice shelves are unrealistic and thus unreliable when assessing the interaction of ice streams and ice shelves. Subsequent work by *Van der Veen and Whillans* [1996] aimed at examining the evolution of ice streams neglects longitudinal deviatoric stresses altogether. Their work, and similar investigations [*Hindmarsh and Le Meur*, 2001; *Le Meur and Hindmarsh*, 2001; *Hindmarsh and Le Meur*, 2002], thus do not elucidate the role of buttressing, which manifests itself through its effect on the longitudinal deviatoric stress at the grounding line. Interestingly, some have cited observations of little or no tensile strain-rate at the grounding line of particular ice streams to indicate that ice-shelf buttressing cannot be important [e.g., *Whillans et al.*, 2001]. However, it is this very lack of tensile strain-rates

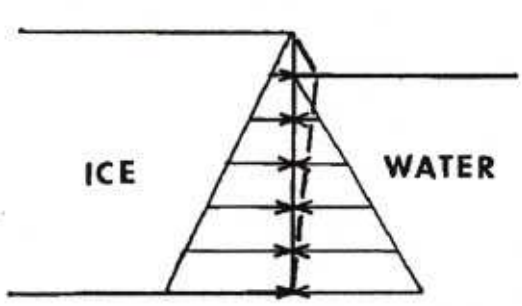

Fig. 1.2. Illustration of the origin of stretching in ice shelves [from *Hughes*, 1998]. Here the large left and right triangles represent the pressure as a function of elevation within the ice and seawater, respectively. The areas of these triangles are the depth-integrated static pressures of the ice and water. The area of the small triangle on the right represents the static integrated pressure difference across the ice front. This static pressure difference requires a compensating stretching force and hence leads to a longitudinal strain rate.

that shows these grounding lines are buttressed. Without buttressing, these sites would have the tensile strain-rate of ice fronts and freely-floating ice shelves.

From the observed thickness and strain-rate fields, *Thomas and MacAyeal* [1982] calculated what they referred to as the 'back force' within the Ross Ice Shelf (RIS). The back force is essentially the difference between the depth-integrated longitudinal deviatoric stress expected if the ice shelf were freely-spreading, and that calculated from the observed strain-rate field. Higher values of back force thus indicate greater buttressing. As shown in figure (1.3), the downstream ends of the ice streams draining into the RIS are clearly buttressed. The work of *MacAyeal et al.* [1987, 1989] showed the importance of buttressing in the vicinity of the Crary Ice Rise. They used a two-dimensional, in plan-view, force-balance model in conjunction with strain-rate measurements to diagnose the forces acting within the study area. From their work it is clear that the strain-rate at the grounding line upstream of the ice rise would be much greater without the drag provided by the ice rise. However, their work was diagnostic in nature, and thus cannot reveal the prognostic consequences, stable or otherwise, of changes in the drag experienced by ice shelves and the resulting buttressing. The same can be said of the more-recent diagnostic work of *Rignot et al.* [2002] and *Schmeltz et al.* [2002] addressing the Pine Island embayment of West Antarctica.

Subsequent work by *MacAyeal* [1992] employed a prognostic model of the whole West Antarctic Ice Sheet, and included thermodynamics, crude sediment dynamics, and both inland and stream/shelf flow regimes. The main goal of this work was to simulate the evolution of WAIS over glacial cycles. The results showed irregular variations in ice volume, with episodes of complete collapse. The resolution of this study was by necessity

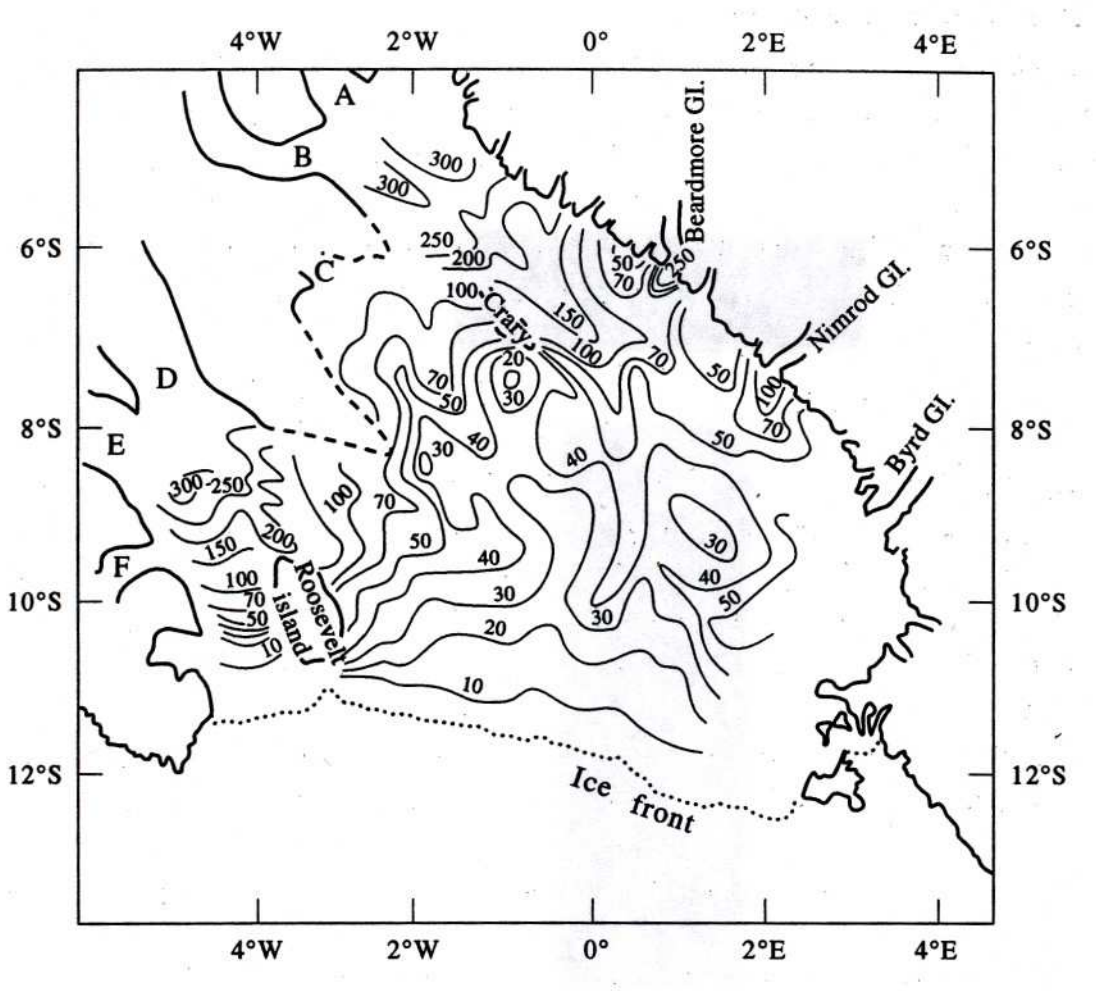

Fig. 1.3. Contour plot showing lines of equal back force as calculated by *Thomas and MacAyeal* [1982]. This back force is measured in MN per unit width of the ice shelf. Effectively, the larger the back force, the more buttressed the ice shelf is. In these units, the total spreading force in the absence of this back force would range from ≈ 300 near the grounding lines to ≈ 50 near the ice front; thus, the back force offsets almost all of the spreading stress in places and must be included to allow accurate calculations almost everywhere.

coarse in space and time. This is unfortunate given the short spatial (order of one ice thickness) and temporal scales within which ice stream and ice shelf dynamics operate [*Bindschadler and Vornberger*, 1998; *Rignot*, 1998; *Joughin et al.*, 1999; *Shepherd et al.*, 2001, 2003]. Given this coarse resolution as well as the complexity of interaction between the thermodynamic, sediment and force-balance components of the model, assessment of the results is difficult and the question of the near-term (millennial or shorter) stability of WAIS remains open.

1.2 Outburst floods and slope-reversal

Glaciers and ice sheets are some of the post powerful agents for geomorphic change [e.g., *Hallet et al.*, 1996; *Cutler et al.*, 2002]. Subglacial water is one of the key ingredients for this geomorphic dynamism. Storage of subglacial water in sufficient quantity can lead, upon release, to flooding events. Present-day examples of such events, sometimes referred to as jokulhlaups, can be exceptionally large and destructive in comparison to 'ordinary' floods, [e.g., *Johannesson*, 2002], although most recent outbursts have been smaller. *Alley et al.* [2003a] hypothesize that larger ice masses, either extant (e.g., Greenland and West Antarctic ice sheets) or otherwise (e.g., Laurentide and Fennoscandian ice sheets), are able to produce even larger outburst flood events.

One of the key features of the outburst flood hypothesis of *Alley et al.* [2003a] is the presence of an overdeepening with closed bathymetric contours, which allows for the trapping and storage of subglacial water. Such overdeepened basins are in evidence today as fjords and sounds as well as still-occupied glacial valleys and basins, and are characterized by long, deep channels terminated by shallow sills.

Clearly, an additional ingredient for creating large outburst floods is the ability to provide a seal for the storage and pressurization of subglacial water. One way to seal the subglacial water system is to have the ice freeze onto the subglacial substrate around the reservoir. A second mechanism is the creation of a reversal in hydrologic gradient by reversing the ice-air surface slope over the sill. *Alley et al.* [2003a] suggested that the localized basal friction experienced as the ice grounds and flows over the sill should produce such surface-slope reversals. Modeling such slope reversals requires the inclusion of longitudinal deviatoric stresses in order to communicate the localized momentum loss through basal drag to the upglacier ice.

1.3 Summary and preview

The consideration of ice-shelf buttressing and surface-slope reversal requires proper treatment of longitudinal-deviatoric stress. The work presented here involves the development and application of a model that includes this stress and can capture the resulting dynamic consequences. Ultimately, the utility of the model lies in its efficiency, wrought through its conceptual simplicity, which allows for a relatively inexpensive examination of the importance of the various parameters inherent to the ice shelves and ice streams.

Chapter 2

Derivation of the momentum balance equation for ice streams and ice shelves

2.1 Introduction

The purpose of this chapter is to derive the momentum balance equation used in chapters (3) and (4) of this dissertation. The road-map from the unadulterated x-directed stress equilibrium equation to the final simplified and nondimensional form involves seven main steps: (i) vertical integration, (ii) lateral integration, (iii) elimination of the pressure, (iv) scaling, (v) introducing constitutive relations, (vi) statement of boundary conditions, and (vii) nondimensionalization. One could shorten the process by starting from the equations of *MacAyeal* [1989], width-integrating, applying lateral boundary conditions, and nondimensionalizing. We take the longer approach in the interest of clarity and completeness. The result is a momentum balance equation appropriate for a thin, channelized flow of ice where shear is isolated within thin boundary layers.

2.2 x-directed stress equilibrium equation

For the flow of ice within glaciers and ice sheets, the inertial terms of the equations of motion [e.g., *Bachelor*, 1967, p. 137] are negligible in comparison to the gravitational body force and the viscous stresses. In this case the equations of motion simplify to a balance of body forces and stress gradients, referred to as the stress equilibrium equations

[*Hooke*, 1998, p. 159]. Here we designate the x-direction as the primary direction of flow. The stress equilibrium equation in this direction is

$$\partial_x \tau_{xx} + \partial_y \tau_{xy} + \partial_z \tau_{xz} = 0 \tag{2.1}$$

where τ_{xx} is the longitudinal stress component, τ_{xy} is the lateral shear stress component, τ_{xz} is the x-directed vertical shear stress component, and $\partial_x \equiv \frac{\partial}{\partial x}$, $\partial_y \equiv \frac{\partial}{\partial y}$, and $\partial_z \equiv \frac{\partial}{\partial z}$ are the longitudinal, lateral and vertical partial derivatives.

2.3 Vertical integration

Integrating equation (2.1) in the vertical (z) direction from the basal surface $z = z_b(x)$ to the upper surface $z = z_s(x)$, i.e., over the thickness $h(x) = z_s - z_b$, yields

$$\begin{aligned} \partial_x \left(h\langle\tau_{xx}\rangle_z\right) + \partial_y \left(h\langle\tau_{xy}\rangle_z\right) &= \tau_{xx}(z_s)\partial_x z_s + \tau_{xy}(z_s)\partial_y z_s - \tau_{xz}(z_s) \\ &\quad -\tau_{xx}(z_b)\partial_x z_b - \tau_{xy}(z_b)\partial_y z_b + \tau_{xz}(z_b) \end{aligned} \tag{2.2}$$

where $\langle\cdot\rangle_z \equiv \frac{1}{h}\int_{z_b}^{z_s} \cdot dz$ is the vertical averaging operator. The right hand side (RHS) of equation (2.2) contains the horizontal components of the traction experienced by the ice at its upper and basal surfaces. The relatively inviscid and low-density atmosphere offers essentially no traction to the ice, and thus a free-surface boundary condition is appropriate at this surface

$$\tau_{xx}(z_s)\partial_x z_s + \tau_{xy}\partial_y z_s - \tau_{xz}(z_s) = 0 \tag{2.3}$$

The appropriate boundary condition to apply at the bed is more nebulous, but we assume here that the traction at this surface is of two forms: (i) glaciostatic and (ii) dynamic. The glaciostatic traction is simply the glaciostatic pressure acting in the x direction against any x-directed component of the basal surface. The dynamic traction or drag is that resulting from motion of the ice over the bed. We express the basal traction as

$$\tau_{xx}(z_b)\partial_x z_b + \tau_{xy}\partial_y z_b - \tau_{xz}(z_b) \quad = \quad -\rho_i g h \partial_x z_b - \begin{cases} \tau_b & \text{grounded} \\ 0 & \text{floating} \end{cases} \tag{2.4}$$

where ρ_i is the density of ice, τ_b is the dynamic basal drag, and g is the gravitational acceleration. Note that the change from grounded to floating conditions includes two effects. The first is the loss of dynamic drag when floating due to the relatively inviscid nature of water. The second is a modification of the glaciostatic term because the ocean and ice pressures must balance at this surface (i.e., buoyancy); the basal surface is then explicitly related to the thickness by this pressure balance such that $z_b = -\frac{\rho_i}{\rho_{sw}} h$, where ρ_{sw} is the density of seawater.

Substituting the boundary conditions (2.3) and (2.4) into equation (2.2) gives

$$\partial_x \left(h \langle \tau_{xx} \rangle_z \right) + \partial_y \left(h \langle \tau_{xy} \rangle_z \right) \quad = \quad \rho_i g h \partial_x z_b + \begin{cases} \tau_b & \text{grounded} \\ 0 & \text{floating} \end{cases} \tag{2.5}$$

2.4 Lateral integration

Integrating equation (2.5) in the lateral or cross-flow (y) direction from the center line at $y = 0$ to the lateral boundary $y = L_y(x)$, i.e. over the half-width $L_y(x)$, yields

$$\partial_x \left(h L_y \langle \langle \tau_{xx} \rangle_z \rangle_y \right) = \left[h \langle \tau_{xx} \rangle_z \partial_x L_y - h \langle \tau_{xy} \rangle_z \right]_{y=L_y} + \left[h \langle \tau_{xy} \rangle_z \right]_{y=0} + \rho_i g h L_y \partial_x z_b + \begin{cases} L_y \langle \tau_b \rangle_y & \text{grounded} \\ 0 & \text{floating} \end{cases} \tag{2.6}$$

where $\langle \cdot \rangle_y \equiv \frac{1}{L_y} \int_0^{L_y} \cdot dy$ is the lateral averaging operator, and the first two terms on the RHS represent the depth-integrated tractions at the lateral boundary and center line, respectively. Note that for the sake of simplicity we have assumed that the thickness and basal elevation are constant in the lateral direction; this is not a bad assumption in the sense that such lateral variations are unlikely to drive the laterally-averaged downstream flow.

At the center line, which is envisioned as a line of symmetry, we specify zero lateral shear

$$\left[h \langle \tau_{xy} \rangle_z \right]_{y=0} = 0 \tag{2.7}$$

At the lateral boundary we specify that the depth-integrated traction be composed similarly to the basal traction, having glaciostatic and dynamic components such that

$$\left[h\langle\tau_{xx}\rangle_z\partial_x L_y - h\langle\tau_{xy}\rangle_z\right]_{y=L_y} = -\frac{\rho_i g}{2}h^2\partial_x L_y + h\tau_y \tag{2.8}$$

Substituting equations (2.7) and (2.8) into equation (2.6) gives

$$\partial_x\left(hL_y\langle\langle\tau_{xx}\rangle_z\rangle_y\right) = \rho_i g h L_y\partial_x z_b - \frac{\rho_i g}{2}h^2\partial_x L_y + h\tau_y + \begin{cases} L_y\langle\tau_b\rangle_y & \text{grounded} \\ 0 & \text{floating} \end{cases} \tag{2.9}$$

2.5 Pressure and the vertical stress equilibrium

We now introduce pressure into the problem. The pressure is defined here in terms of the normal stresses such that

$$p \equiv -\frac{1}{3}\left(\tau_{xx} + \tau_{yy} + \tau_{zz}\right) \tag{2.10}$$

where τ_{yy} and τ_{zz} are the normal stresses in the lateral and vertical directions, respectively. Here we have adopted the convention that a tension is positive, and we see that the pressure, a compressive quantity, is defined as the negative arithmetic mean of the normal stresses. Given this definition we may decompose the normal stresses into mean

and deviatoric components,

$$\tau_{xx} = \tau'_{xx} - p \tag{2.11}$$

$$\tau_{yy} = \tau'_{yy} - p \tag{2.12}$$

$$\tau_{zz} = \tau'_{zz} - p \tag{2.13}$$

where the prime denotes the deviator. This definition implies, in conjunction with the definition of pressure (equation 2.10), that the deviatoric stresses sum to zero,

$$\tau'_{xx} + \tau'_{yy} + \tau'_{zz} = 0 \tag{2.14}$$

Substituting the decomposed longitudinal stress into equation (2.9) gives

$$\partial_x \left(hL_y \langle \langle \tau'_{xx} - p \rangle_z \rangle_y \right) = \rho_i g h L_y \partial_x z_b - \frac{\rho_i g}{2} h^2 \partial_x L_y + h\tau_y + \begin{cases} L_y \langle \tau_b \rangle_y & \text{grounded} \\ 0 & \text{floating} \end{cases} \tag{2.15}$$

To eliminate the pressure p from this horizontal-momentum-balance equation we now use the vertical momentum balance, in the form of the vertical-stress-equilibrium equation

$$\partial_x \tau_{xz} + \partial_y \tau_{yz} + \partial_z \tau_{zz} = \rho_i g \tag{2.16}$$

where τ_{yz} is vertical shear stress in the lateral direction and τ_{zz} is the vertical normal stress. Integration of equation (2.16) in the vertical from an arbitrary elevation z to the surface $z_s(x)$ yields an expression for the vertical normal stress as a function of elevation

$$\begin{aligned}\tau_{zz}(z) &= -\rho_i g\,(z_s - z) \\ &\quad +\partial_x\left(\int_z^{z_s}\tau_{xz}dz\right)+\partial_y\left(\int_z^{z_s}\tau_{yz}dx\right) \\ &\quad -\tau_{xz}(z_s)\partial_x z_s - \tau_{yz}(z_s)\partial_y z_s + \tau_{zz}(z_s) \qquad (2.17)\end{aligned}$$

As with the horizontal traction we assume that the vertical traction at the upper surface, that provided by the atmosphere, is zero,

$$\tau_{xz}(z_s)\partial_x z_s + \tau_{yz}(z_s)\partial_y z_s - \tau_{zz}(z_s) = 0 \qquad (2.18)$$

Using this boundary condition in equation (2.17) yields

$$\tau_{zz}(z) = -\rho_i g\,(z_s - z) + \partial_x\left(\int_z^{z_s}\tau_{xz}dz\right)+\partial_y\left(\int_z^{z_s}\tau_{yz}dx\right) \qquad (2.19)$$

Inserting the decomposed version of the vertical normal stress and using the fact that the deviators sum to zero yields

$$p(z) = \rho_i g\,(z_s - z) - \tau'_{xx} - \tau'_{yy} - \partial_x\left(\int_z^{z_s}\tau_{xz}dz\right) - \partial_y\left(\int_z^{z_s}\tau_{yz}dx\right) \qquad (2.20)$$

The integral terms on the RHS of this equation are awkward. They are so awkward, in fact, that we will now endeavor to banish them. We do this by introducing rheology and

then using the scales of the problem to show that these ugly terms are, for the problem at hand, negligible.

We assume that the ice is flowing via power-law creep, represented in nonlinear viscous form as

$$\underline{\tau}' \equiv 2\nu\underline{\dot{\epsilon}} \tag{2.21}$$

where $\underline{\tau}'$ and $\underline{\dot{\epsilon}}$ are the the deviatoric stress and strain-rate tensors, respectively, defined as

$$\underline{\tau}' \equiv \begin{bmatrix} \tau'_{xx} & \tau_{xy} & \tau_{xz} \\ \tau_{xy} & \tau'_{yy} & \tau_{yz} \\ \tau_{xz} & \tau_{yz} & \tau'_{zz} \end{bmatrix} \tag{2.22}$$

and

$$\underline{\dot{\epsilon}} \equiv \begin{bmatrix} \dot{\epsilon}_{xx} & \dot{\epsilon}_{xy} & \dot{\epsilon}_{xz} \\ \dot{\epsilon}_{xy} & \dot{\epsilon}_{yy} & \dot{\epsilon}_{yz} \\ \dot{\epsilon}_{xz} & \dot{\epsilon}_{yz} & \dot{\epsilon}_{zz} \end{bmatrix} \equiv \begin{bmatrix} \partial_x u & \frac{1}{2}\left(\partial_y u + \partial_x v\right) & \frac{1}{2}\left(\partial_z u + \partial_x w\right) \\ \frac{1}{2}\left(\partial_y u + \partial_x v\right) & \partial_y v & \frac{1}{2}\left(\partial_z v + \partial_y w\right) \\ \frac{1}{2}\left(\partial_z u + \partial_x w\right) & \frac{1}{2}\left(\partial_z v + \partial_y w\right) & \partial_z w \end{bmatrix} \tag{2.23}$$

where u, v, and w are the longitudinal, lateral and vertical flow velocities, respectively. ν is the strain-rate-dependent viscosity,

$$\nu \equiv \frac{B_i}{2}\left(\dot{\epsilon}_{xx}^2 + \dot{\epsilon}_{yy}^2 + \dot{\epsilon}_{xx}\dot{\epsilon}_{yy} + \dot{\epsilon}_{xy}^2 + \dot{\epsilon}_{xz}^2 + \dot{\epsilon}_{yz}^2\right)^{\frac{1-n}{2n}} \tag{2.24}$$

where B_i is the ice hardness, $n = 3$ is the flow-law exponent, and where we have employed the incompressibility condition

$$\dot{\epsilon}_{xx} + \dot{\epsilon}_{yy} + \dot{\epsilon}_{zz} \quad = \quad 0 \tag{2.25}$$

to eliminate the vertical strain-rate component $\dot{\epsilon}_{zz}$ from the definition of the viscosity. Incompressibility is a good assumption for ice beyond seismic time-scales [e.g., *Hooke*, 1998, p. 7].

2.6 Scaling

Let us now introduce scales that will help in the simplification of the equation for pressure (equation (2.20)). To start, let the coordinates scale as

$$\left[\begin{array}{ccc} x & y & z \end{array} \right] \quad = \quad O\left(\left[\begin{array}{ccc} L_x & L_y & H \end{array} \right] \right) \tag{2.26}$$

where L_x, L_y, and H are the longitudinal, lateral and vertical length scales. Let the velocity gradients scale as

$$\left[\begin{array}{ccc} \partial_x u & \partial_y u & \partial_z u \\ \partial_x v & \partial_y v & \partial_z v \\ \partial_x w & \partial_y w & \partial_z w \end{array} \right] \quad = \quad O\left(\left[\begin{array}{ccc} \frac{U}{L_x} & \frac{\delta_y U}{L_y} & \frac{\delta_z U}{H} \\ \frac{\delta_x V}{L_x} & \frac{\delta_y V}{L_y} & \frac{\delta_z V}{H} \\ \frac{\delta_x W}{L_x} & \frac{\delta_y W}{L_y} & \left(\frac{U}{L_x} + \frac{\delta_y V}{L_y} \right) \end{array} \right] \right) \tag{2.27}$$

where the $\delta_*()$ notation implies the variation in the quantity $()$ over the $*^{th}$ length scale. In the case of the longitudinal gradient in longitudinal velocity $\partial_x u$, by setting $\delta_x U = U$

we imply a variation in u in the x direction of the same order as the velocity scale U. Note that the scales for the remaining velocity gradients are more interesting than simply a velocity scale over a length scale. This is because we expect the scales of velocity changes to be different over the different length scales. For example, compare the scales for $\partial_x u$ and $\partial_z u$; we allow for a total velocity change of U over the longitudinal length scale of L_x, but because we are looking at ice flowing over a weak bed we expect only a change of $\delta_z U << U$ over the thickness scale H.

In the present studies we restrict ourselves to thin, channelized ice flow with little internal shear and with negligible vertical or lateral velocity. This in effect restricts our consideration to a kind of plug flow, in that the momentum flux to the bed and to the side of the channel is isolated in thin[1] boundary layers. In this flow regime the only strain-rate of note within the main flow of ice is longitudinal strain-rate.

For this thin-ice, plug-flow regime to be appropriate the scales must satisfy the following conditions. Thin ice implies

$$\left[\begin{array}{cc} \frac{H}{L_x} & \frac{H}{L_y} \end{array} \right] \ll 1 \tag{2.28}$$

Channelized flow with negligible lateral or vertical velocity requires

$$\left[\begin{array}{ccccc} \frac{\delta_x V}{U} & \frac{\delta_y V}{U} & \frac{\delta_z V}{U} & \frac{\delta_x W}{U} & \frac{\delta_y W}{U} \end{array} \right] \ll 1 \tag{2.29}$$

[1]We consider a thin boundary basal (lateral) boundary layer to be one whose size is much smaller than the channel thickness (width). For example, for an ice thickness of 1 km, a thin basal boundary layer would be on the order of 10 m or less in thickness.

Lastly, neglecting lateral and vertical shear requires

$$\begin{bmatrix} \frac{\delta_y U}{U} & \frac{\delta_z U}{U} \end{bmatrix} < 2 \begin{bmatrix} \frac{L_y}{L_x} & \frac{H}{L_x} \end{bmatrix} \tag{2.30}$$

With these scales the sizes of the two integral terms in the RHS of equation (2.20) relative to the longitudinal deviatoric stress are respectively

$$\begin{bmatrix} \frac{\partial_x \int_z^{z_s} \tau_{xz} dz}{\tau'_{xx}} \\ \frac{\partial_y \int_z^{z_s} \tau_{yz} dz}{\tau'_{xx}} \end{bmatrix} = O\left(\frac{1}{2} \begin{bmatrix} \left(\frac{\delta_z U}{U} + \frac{\delta_x W}{U} \frac{H}{L_x} \right) \\ \left(\frac{\delta_z V}{U} \frac{L_x}{L_y} + \frac{\delta_y W}{U} \frac{H}{L_y} \frac{L_x}{L_y} \right) \end{bmatrix} \right) \tag{2.31}$$

Because these ratios are small we can safely drop those awkward integral terms from the RHS of equation (2.20). In addition we can drop the τ'_{yy} term because its scale is small relative to τ'_{xx}. Thus equation (2.20) simplifies to

$$p(z) = \rho_i g \left(z_s - z \right) - \tau'_{xx} \tag{2.32}$$

The two terms on the RHS are sometimes referred to as the static and dynamic components of pressure [2]

Width and depth integration of the above expression for the pressure yields

$$L_y h \langle \langle p \rangle_z \rangle_y = \frac{\rho_i g}{2} L_y h^2 - L_y h \langle \langle \tau'_{xx} \rangle_z \rangle_y \tag{2.33}$$

[2] Comparing the sizes of these components in a depth averaged sense requires the introduction of a rheological relation, as well as appropriate scales. It so happens that for the scales used in chapters (3) and (4) the scale of static pressure is roughly from 1 to 20× that for the dynamic pressure.

Using this expression in the width- and depth-integrated x-directed momentum equation (equation (2.15)) yields

$$\partial_x \left(2L_y h\langle\langle \tau'_{xx}\rangle_z\rangle_y\right) = L_y \frac{\rho_i g}{2}\partial_x h^2 + L_y \rho_i g h \partial_x z_b + h\tau_y + \begin{cases} L_y\langle\tau_b\rangle_y & \text{grounded} \\ 0 & \text{floating} \end{cases} \tag{2.34}$$

If we assume that the relative longitudinal change in half-width is small (i.e. the width changes slowly along flow) then dividing by L_y and rearranging gives

$$\partial_x \left(2h\langle\langle \tau'_{xx}\rangle_z\rangle_y - \frac{\rho_i g}{2}h^2\right) = \rho_i g h \partial_x z_b + \frac{h}{L_y}\tau_y + \begin{cases} \langle\tau_b\rangle_y & \text{grounded} \\ 0 & \text{floating} \end{cases} \tag{2.35}$$

Note that the expression within the x-derivative on the left-hand side (LHS) is depth-integrated, width-averaged longitudinal normal stress,

$$h\langle\langle \tau_{xx}\rangle_z\rangle_y = 2h\langle\langle \tau'_{xx}\rangle_z\rangle_y - \frac{\rho_i g}{2}h^2 \tag{2.36}$$

2.7 Constitutive relations

To relate the longitudinal deviatoric stress to velocity we now insert the viscous rheology of equation (2.21) into equation (2.35)

$$\partial_x \left(4h\nu\partial_x u - \frac{\rho_i g}{2}h^2\right) = \rho_i g h \partial_x z_b + \frac{h}{L_y}\tau_y + \begin{cases} \langle\tau_b\rangle_y & \text{grounded} \\ 0 & \text{floating} \end{cases} \tag{2.37}$$

where we have used the fact that the lateral and vertical variations of u are negligible to drop the vertical and lateral averaging operators acting on the longitudinal deviatoric stress. Similarly, because the longitudinal strain-rate is the only non-negligible strain rate component, the viscosity definition (equation (2.21) simplifies to

$$\nu = \frac{\langle\langle B_i \rangle_z \rangle_y}{2} |\partial_x u|^{\frac{1-n}{n}} \tag{2.38}$$

where $\langle\langle B_i \rangle_z \rangle_y$ is the depth and width averaged ice hardness.

With the viscous rheology we relate the flow, or more correctly the strain-rate, to the longitudinal stress deviator. We now need to relate the lateral and basal drag terms in equation (2.37) to the flow. Both drags are assumed to be derived from shearing isolated within thin boundary layers. It therefore seems appropriate to assume that the stress state within these boundary layers is dominated by a single shear stress component; τ_{xy} for the lateral shear zone, and τ_{xz} for the basal shear zone. For the lateral shear zone the material undergoing shear is the ice, for which the power-law viscous rheology of equations (2.21) and (2.24) is appropriate. For the basal shear zone the material being sheared is assumed to be relatively weak material such as a soft sediment (e.g., till), water, or even ice undergoing enhanced deformation [*Alley et al.*, 1986; *Weertman*, 1964]. For the rheology of this material we also use a power-law viscous relation, but leave the power-law exponent arbitrary, at least for the moment. Given these considerations, the lateral and basal drags are related to the main flow within the channel using the

following expressions

$$\tau_y = B_s \left(\frac{u}{2y_s} \right)^{\frac{1}{n}} \tag{2.39}$$

$$\langle \tau_b \rangle_y = \langle B_b \rangle_y \left(\frac{u}{2h_b} \right)^{\frac{1}{m}} \tag{2.40}$$

where B_s is the ice hardness within the lateral boundary layer, y_s is the width of this lateral boundary layer, $\langle B_b \rangle_y$ is the hardness of the basal layer, h_b is the thickness of this shear zone, and m is the arbitrary flow-law exponent for the basal material.

These expressions in conjunction with equation (2.37) give us an equation for the x-directed momentum balance in terms of the thickness, h, width, L_y, velocity, u, and the various constitutive parameters

$$\partial_x \left(4h\nu\partial_x u - \frac{\rho_i g}{2} h^2 \right) = \rho_i g h \partial_x z_b + \frac{h B_s}{L_y \left(2y_s\right)^{\frac{1}{n}}} u^{\frac{1}{n}} + \begin{cases} \dfrac{B_b}{(2h_b)^{\frac{1}{m}}} u^{\frac{1}{m}} & \text{grounded} \\ 0 & \text{floating} \end{cases} \tag{2.41}$$

2.8 Boundary conditions

Equation (2.41) is a second-order differential equation in $u(x)$, and this suggests that its solution for u will require two boundary conditions. We in fact impose an essential boundary condition at the upstream end, $x = 0$, and a natural one at the downstream end, $x = L_x$.

At the upstream end we specify the velocity,

$$u(x = 0) = u_0 \tag{2.42}$$

At the downstream end we have a more interesting situation. Here the depth-integrated, width-averaged, longitudinal stress,

$$\left[h\langle\langle\tau_{xx}\rangle_z\rangle_y\right]_{x=L_x} = \left[4h\nu\partial_x u - \frac{\rho_i g}{2}h^2\right]_{x=L_x} \tag{2.43}$$

is prescribed. We envision two end-members for this stress-state: (i) unbuttressed and (ii) fully buttressed. Here we define buttressed as experiencing a reduction in the tensile deviatoric stress experienced at an ice front or communicated by a freely floating ice shelf.

The first end-member is that appropriate for this point either being an ice front or the point at which ice flows into a freely-floating ice shelf. In this unbuttressed case the depth-integrated, width-averaged longitudinal stress is that provided by the ocean, either directly onto the vertical face at $x = L_x$ or indirectly on the appended freely-floating ice shelf. In both the direct and indirect cases the depth-integrated longitudinal stress provided by the ocean is, to good approximation given the small viscosity of water relative to ice, the depth integrated hydrostatic ocean pressure,

$$\left[4h\nu\partial_x u - \frac{\rho_i g}{2}h^2\right]_{x=L_x} = \left[-\frac{\rho_{sw} g}{2}z_b^2\right]_{x=L_x} \tag{2.44}$$

where sea level is set at $z = 0$. It can be shown that this condition implies a positive or tensile strain-rate because

$$\frac{\rho_i g}{2}h^2 - \frac{\rho_{sw} g}{2}z_b^2 \geq \frac{\rho_i g}{2}h^2\left(1 - \frac{\rho_i}{\rho_{sw}}\right) \tag{2.45}$$

The term on the RHS is the maximum depth-integrated static pressure difference between the ice and the ocean for ice that is either grounded at a depth $-z_r = -z_b < -\frac{\rho_i}{\rho_{sw}}h$ or floating, in which case $-z_r > z_b = -\frac{\rho_i}{\rho_{sw}}h$, where $-z_r$ is the depth the sea-water.

The second end-member for the downstream stress state considered here is one in which the strain-rate at this point is zero,

$$[4h\nu\partial_x u]_{x=L_x} = 0 \tag{2.46}$$

This is what we refer to as the fully buttressed case. It is buttressed in the sense that the tensile condition we see in (2.44) is completely nullified. Here the buttressing is caused by frictional drag on the ice shelf extending beyond $x = L_x$, which reduces the ability of this shelf to communicate the tensile deviatoric stress seen in condition (2.44) to the point $x = L_x$. One can in fact envision super-buttressed states where the longitudinal strain rate is compressive at the downglacier end, but we do not consider these extreme cases here.

To allow for states that fall somewhere between the fully buttressed and unbuttressed conditions of (2.46) and (2.44), we define a buttressing parameter f such that if $f = 1$ a fully buttressed condition is imposed, and if $f = 0$ an unbuttressed condition is imposed, using the following linear combination of the two conditions,

$$\left[4h\nu\partial_x u - \frac{\rho_i g}{2}h^2\right]_{x=L_x} = \left[-f\frac{\rho_i g}{2}h^2 - (1-f)\frac{\rho_{sw} g}{2}z_b^2\right]_{x=L_x} \tag{2.47}$$

2.9 Nondimensionalizing

To isolate the key parameters we now convert equation (2.41), its constitutive relations and its boundary conditions into nondimensional forms. We restate the dimensional equations,

$$\partial_x \left(4h\nu\partial_x u - \frac{\rho_i g}{2}h^2\right) = \rho_i g h \partial_x z_b + \frac{h}{L_y}\tau_y(u) + \begin{cases} \tau_b(u) & \text{grounded} \\ 0 & \text{floating} \end{cases} \tag{2.48}$$

$$u(x=0) = u_0 \tag{2.49}$$

$$\left[4h\nu\partial_x u - \frac{\rho_i g}{2}h^2\right]_{x=L_x} = \left[-f\frac{\rho_i g}{2}h^2 - (1-f)\frac{\rho_{sw} g}{2}z_b^2\right]_{x=L_x} \tag{2.50}$$

where

$$\nu \equiv \frac{\langle\langle B_i\rangle_z\rangle_y}{2}\left|\partial_x u\right|^{\frac{1-n}{n}} \tag{2.51}$$

$$\tau_y \equiv B_s\left(\frac{u}{2y_s}\right)^{\frac{1}{n}} \tag{2.52}$$

$$\tau_b \equiv B_b\left(\frac{u}{2h_b}\right)^{\frac{1}{m}} \tag{2.53}$$

Now let us introduce the following scales

$$x \mapsto L_x x \tag{2.54}$$

$$h \mapsto Hh \tag{2.55}$$

$$u \mapsto Uu \tag{2.56}$$

$$\langle\langle B_i\rangle_z\rangle_y \mapsto B_i \tag{2.57}$$

$$\nu \mapsto \frac{B_i}{2}\left(\frac{U}{L_x}\right)^{\frac{1-n}{n}}\nu \tag{2.58}$$

$$z_b \mapsto Hz_b \tag{2.59}$$

$$L_y \mapsto L_y \tag{2.60}$$

$$\tau_y(u) \mapsto \tau_y u^{\frac{1}{n}} \tag{2.61}$$

$$\tau_b(u) \mapsto \tau_b u^{\frac{1}{m}} \tag{2.62}$$

$$u_0 \mapsto Uu_0 \tag{2.63}$$

where

$$\nu \equiv |\partial_x u|^{\frac{1-n}{n}} \tag{2.64}$$

is the nondimensional viscosity. We treat the scales L_x, H, U, B_i, L_y, τ_y, and τ_b, along with g, ρ_i, and ρ_{sw}, as constants in x. Given these scales, the x-directed momentum

balance problem may be expressed in the following nondimensional form

$$\partial_x\left(2h\nu\partial_x u - \frac{A}{2}h^2\right) = Ah\partial_x z_b + G_s h u^{\frac{1}{n}} + \begin{cases} G_b u^{\frac{1}{m}} & \text{grounded} \\ 0 & \text{floating} \end{cases} \tag{2.65}$$

$$u(x=0) = u_0 \tag{2.66}$$

$$\left[2h\nu\partial_x u - \frac{A}{2}h^2\right]_{x=1} = \left[-f\frac{A}{2}h^2 - (1-f)\,r_{sw}\frac{A}{2}z_b^2\right]_{x=1} \tag{2.67}$$

$$\nu = |\partial_x u|^{\frac{1-n}{n}} \tag{2.68}$$

where we have defined four dimensionless numbers

$$A \equiv \frac{\rho_i g H}{B_i\left(\frac{U}{L_x}\right)^{\frac{1}{n}}} \tag{2.69}$$

$$G_s \equiv \frac{L_x \tau_y}{L_y B_i\left(\frac{U}{L_x}\right)^{\frac{1}{n}}} \tag{2.70}$$

$$G_b \equiv \frac{L_x \tau_b}{H B_i\left(\frac{U}{L_x}\right)^{\frac{1}{n}}} \tag{2.71}$$

$$r_{sw} \equiv \frac{\rho_{sw}}{\rho_i} \tag{2.72}$$

The last of these numbers is simply the density of seawater relative to ice. The first three numbers, A, G_s and G_b, measure respectively the strength of the driving stress, the side drag, and the basal drag relative to the strength of the gradient in the depth-integrated longitudinal deviatoric stress.

Equations (2.65)-(2.68) are perhaps the simplest possible statement of the momentum balance of an ice-stream/shelf system that includes the essential physics of side

drag, basal drag, longitudinal deviatoric stresses, and ice-shelf buttressing. In formulating these equations in terms of the dimensionless numbers A, G_s, and G_b, we have made it particularly simple to evaluate a wide range of possible physical situations, as in the next two chapters.

Chapter 3

When buttressing matters: a sensitivity study

3.1 Introduction

Ice streams are regions of concentrated fast flow relative to the surrounding ice. As such, these regions represent efficient pathways of mass flux from the interiors of ice sheets. Thus, changes in ice streams have the potential of producing major changes in ice-sheet mass balance and sea-level. Modern ice streams almost invariably flow into floating extensions called ice shelves. An open issue in glaciology is the extent to which changes in the ability of these ice shelves to buttress their ice streams will affect those ice streams.

Here we examine the sensitivity of stream/shelf systems to changes in downstream buttressing. We do this using a non-dimensional model of the coupled mass and momentum balance of a stream/shelf system.

3.2 Model Description

For this problem we adopt the geometry shown in figure (3.1). The dimensional scales for the problem are listed in table (3.1). All variables are nondimensional unless otherwise noted. The flow is from left to right along the flow direction x from $x = 0$ to $x = 1$. The stream/shelf channel is of unit width. The elevation of the channel's bed z_r

is specified as

$$z_r(x) = -\frac{1}{r_{sw}} + \beta\,(x-1) \tag{3.1}$$

where $r_{sw} = \frac{\rho_{sw}}{\rho_i}$ is ratio of the density of seawater to ice, and β is the gradient in bed elevation. Note that given this bed elevation, the flotation thickness h_f is

$$h_f(x) = 1 + r_{sw}\beta\,(1-x) \tag{3.2}$$

This is the maximum thickness for floating ice, such that the ice is floating if $h \leq h_f$ and the ice is grounded if $h > h_f$, where $h = h(x,t)$ is the ice thickness.

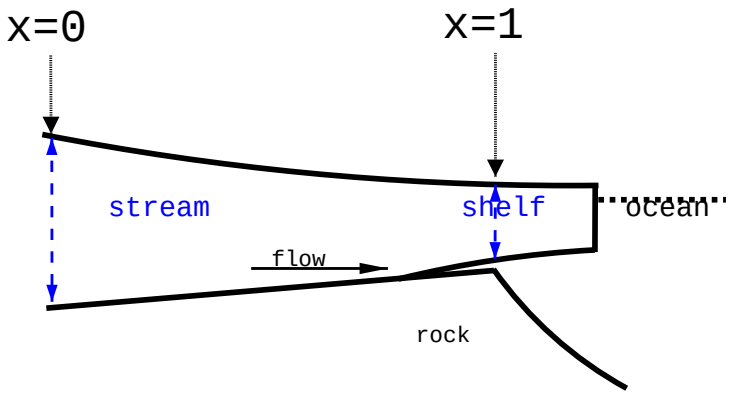

Fig. 3.1. Schematic geometry

3.2.1 governing equations and boundary conditions

We model the momentum balance using equation (2.65), derived in chapter (2), modified here to take account of the specified channel bed elevation:

$$\partial_x \left(2h\nu\partial_x u - \frac{A}{2}h^2 \right) = G_s h u^{\frac{1}{n}} + \begin{cases} A\beta h + G_b u^{\frac{1}{m}} & h > h_f \\ -\frac{A}{2r_{sw}}\partial_x h^2 & h \leq h_f \end{cases} \tag{3.3}$$

This non-dimensional, width-averaged and depth-integrated stress-equilibrium equation is appropriate for thin, channelized flow within ice streams and shelves. Here $u = u(x,t)$ is the flow velocity, ∂_x is the x-directed derivative, $z_b = z_b(x,t)$ is elevation of the base of the ice, $n = 3$ is the flow-law exponent for ice, and m is the flow-law exponent for the basal material. ν is the strain-rate dependent viscosity, defined as

$$\nu\left(\partial_x u\right) \equiv \left|\partial_x u\right|^{\frac{1-n}{n}} \tag{3.4}$$

The non-dimensional parameters A, G_s and G_b are determined from the scales adopted as follows

$$A \equiv \frac{\rho_i g H}{B_i \left(\frac{U}{L_x}\right)^{\frac{1}{n}}} \tag{3.5}$$

$$G_s \equiv \frac{L_x \tau_y}{L_y B_i \left(\frac{U}{L_x}\right)^{\frac{1}{n}}} \tag{3.6}$$

$$G_b \equiv \frac{L_x \tau_b}{H B_i \left(\frac{U}{L_x}\right)^{\frac{1}{n}}} \tag{3.7}$$

where H is the thickness scale, L_x is the longitudinal length scale, L_y is the lateral or width length scale, B_i is the ice hardness parameter, U is the velocity scale, τ_y is the lateral shear-stress scale, and τ_b is the basal shear-stress scale. The non-dimensional parameters A, G_s, and G_b measure the respective strengths of the driving stress, lateral shear stress and basal shear stress relative to the stress required to produce the longitudinal strain rate $\frac{U}{L_x}$.

Two boundary conditions are applied to the momentum balance, one at each end of the domain. At the upstream end ($x = 0$) the velocity is a prescribed constant,

$$u(0,t) = u_0 \tag{3.8}$$

The second boundary condition is

$$\left[2h\nu\partial_x u - \frac{A}{2}h^2\right]_{x=1} = \left[-f\frac{A}{2}h^2 - (1-f)\,r_{sw}\frac{A}{2}z_b^2\right]_{x=1} \tag{3.9}$$

where $r_{sw} = \frac{\rho_{sw}}{\rho_i}$ is the ratio of the seawater density to ice density and f is the buttressing parameter. When $f = 0$, the boundary condition is that appropriate for an appended free-floating ice shelf [*Weertman*, 1974]. For such an ice shelf the depth-integrated seawater pressure acting on the ice in the vertical plane perpendicular to the x direction must be balanced by the depth-integrated longitudinal stress at the point of attachment ($x = 1$). This stress is the sum of the depth-integrated glaciostatic pressure and the depth-integrated viscous stress. In the case of the appended free-floating ice shelf, the

difference between the depth-integrated glaciostatic and hydrostatic pressures will always be positive, thus requiring viscous stretching to balance the forces. When $f = 1$, no static pressure difference is permitted and the strain-rate is therefore zero. This is appropriate for an appended ice shelf that dissipates through lateral drag or localized basal drag the force producing the strain-rate in the $f = 0$ case. This $f = 1$ case we refer to as fully buttressed. The $f = 0$ case we refer to as unbuttressed. Any value of f between these two cases is partially buttressed (the overbuttressed case, where $f > 1$, is not considered here).

The mass balance of the system is governed by the equation

$$\partial_t h = -\partial_x (uh) \tag{3.10}$$

where accumulation is neglected and t is the non-dimensional time coordinate, whose dimensional scale is T. Equation (3.10) is derived from continuity and states that the time-rate-of-change in thickness is dictated by the convergence of depth-integrated advective mass-flux.

The thickness at the upstream end is prescribed and serves as the one boundary condition on the mass balance,

$$h(0, t) = h_0 \tag{3.11}$$

3.3 Experiments and Results

Our goal is to assess the sensitivity of an ice-stream/ice-shelf system to changes in the buttressing. To this end, the aforementioned equations are discretized to form

a numerical model suitable for simulating the dynamics of such a system. The spatial discretization uses linear finite elements. The temporal discretization uses semi-implicit finite differencing. Appendix (B) gives the details of the what we believe is a novel (in the context of computational glaciology) Petrov-Galerkin approach employed for the discretization of the evolution equation (3.10).

In all of the numerical experiments conducted here an initial steady state is found that is appropriate for $f = 0.5$ (50% buttressing). We then set $f = 0$ (unbuttressed) and let the system evolve to a new steady-state. Table (3.2) lists the parameter values adopted for each experiment. One experiment was designated the reference experiment. The values chosen for this reference experiment are roughly appropriate for Pine Island Glacier (P.I.G.). The purpose of the remaining experiments is to show the sensitivity of the results to our particular choice of parameter values. The results of this sensitivity study are listed in table (3.3).

Figure (3.2) shows the initial and final states for the reference experiment. The removal of buttressesing produces a marked increase in velocity at the downstream end. This puts the system out of balance, and thinning ensues until a new steady-state is achieved. The downstream end experiences a net relative thinning of over 25%. The region that experienced over 10% relative thinning extends more than 30% upstream. Evolution of the thickness and velocity profiles is shown in figure (3.3). The bulk of the evolution is accomplished within the first unit of non-dimensional time, as can be seen most clearly in the evolution of the grounding line shown in figure (3.4). Also shown in this figure is the evolution of the integrated volume of ice above flotation (VAF). It is the loss of this ice to the ocean that would directly contribute to sea-level rise. The

grounding line retreated about 18% the domain length in total, which would correspond to an 18 km retreat given a 100 km length scale. The net loss in VAF is 0.11 or roughly one third of the initial value of 0.342; this would correspond to roughly 300 km^3 of ice (or 1mm sea-level equivalent) added to the ocean given length, thickness and width scales of 100, 1, and 3 km respectively.

Table (3.3) shows how moderate changes in the parameter values chosen for the reference experiment would affect the primary results. Note that changes imposed leave the parameter values within the ranges corresponding to glaciologically reasonable scales. In all of these sensitivity experiments the results are qualitatively the same as the reference experiment. However, the experiments show several interesting departures from the reference case. One important result of the sensitivity experiments is that an increase in the strength of side drag, as measured by G_s, results in a modest decrease in the grounding line retreat and loss of VAF. This suggests that, all other things being equal, changes in buttressing matter less to systems with stronger side drag. Increasing the relative strength of the driving stress, as measured by A, increases the grounding line retreat and percentage loss of VAF. This suggests that systems with higher driving stress (i.e., depth-integrated glaciostatic pressure gradient) should be expected to be more sensitive to changes in buttressing relative to systems with lower driving stress. Increasing the basal drag, as measured by G_b, increases the loss of VAF by some 10% relative to the reference case. This suggests that, in terms of VAF loss and thus sea-level rise, buttressing changes matter more to systems with stronger basal drag.

3.4 Conclusions

The numerical experiments indicate that a reduction in buttressing results in a notable grounding line retreat and loss in the volume of ice above flotation. They also show that the response extends far upstream from where the buttressing change was imposed. In fact, the upstream extent of the response we estimate is likely a minimum given that we hold the upstream velocity and thickness (and thus the flux) constant in time. Without this restriction, we expect the thinning would continue upstream beyond $x = 0$ in a manner similar to a kinematic wave [*Kamb*, 1964; *Alley and Whillans*, 1984]. The results are also conservative in light of our neglect of an accumulation term in equation (3.10), because as the ice ungrounds and exposes the basal surface to ocean water this surface is likely to experience substantial melting [*Jacobs et al.*, 1996]. This feedback, which would represent the introduction of a strong mass-loss to the system, would tend to augment the grounding line retreat and loss of volume above flotation. In addition our choice of unbuttressing from an initial state of 50% buttressing is likely conservative for some ice streams, such as Whillans ice stream (formerly called Ice Stream B), where the stress state has been diagnosed as essentially 100% buttressed at present [*Whillans and Van der Veen*, 1993].

The sensitivity experiments indicate a greater sensitivity to changes in buttressing for those systems with weaker side drag, larger basal drag, or larger driving stress strength, as measured by the non-dimensional numbers G_s, G_b and A, respectively. Thus with all other things being equal, the wider an ice stream is, or the 'stickier' its bed, or the larger its driving stress, the more sensitive it will be to perturbations in buttressing.

The standard set of parameter values chosen here is appropriate for Pine Island Glacier. Rutford Ice Stream possesses a similarly high driving stress and high basal drag and thus might be expected to show similar sensitivity to buttressing changes. The Siple Coast ice streams are generally lower in driving stress, and might therefore be considered less susceptible to buttressing-induced variations. However, some of these ice streams are wider at the mouth than Pine Island Glacier and Rutford Ice Stream, which by itself would suggest greater sensitivity. Thus, we cannot rule out significant sensitivity of the Siple Coast ice streams to buttressing change, and we suggest that a suite of experiments with parameter values appropriate for Siple Coast ice streams is in order.

Table 3.1. Values of scales, constants and parameters.

Scale, constant or parameter	Value
ρ_i	9.17×10^2 kg m^{-3}
ρ_{sw}	1.028×10^3 kg m^{-3}
g	9.81 m s^{-2}
n	3
m	1
H	1×10^3 m
L_x	1×10^5 m
L_y	2×10^4 m
U	7.6×10^{-5} ms^{-1}
B_i	2×10^8 Pa s$^{1/3}$
τ_b	7.310^5 Pa
τ_y	5.5×10^5 Pa
$r_{sw} = \frac{\rho_{sw}}{\rho_i}$	1.12
$T = L_x/U$	1.3×10^9 s = 41 years
$A = \frac{\rho_i g H}{B_i \left(\frac{U}{L_x}\right)^{\frac{1}{n}}}$	50
$G_s = \frac{L_x \tau_y}{L_y B_i \left(\frac{U}{L_x}\right)^{\frac{1}{n}}}$	15
$G_b = \frac{L_x \tau_b}{H B_i \left(\frac{U}{L_x}\right)^{\frac{1}{n}}}$	40
β	0.3
h_0	1.9
u_0	$\frac{1}{1.9} \approx 0.53$

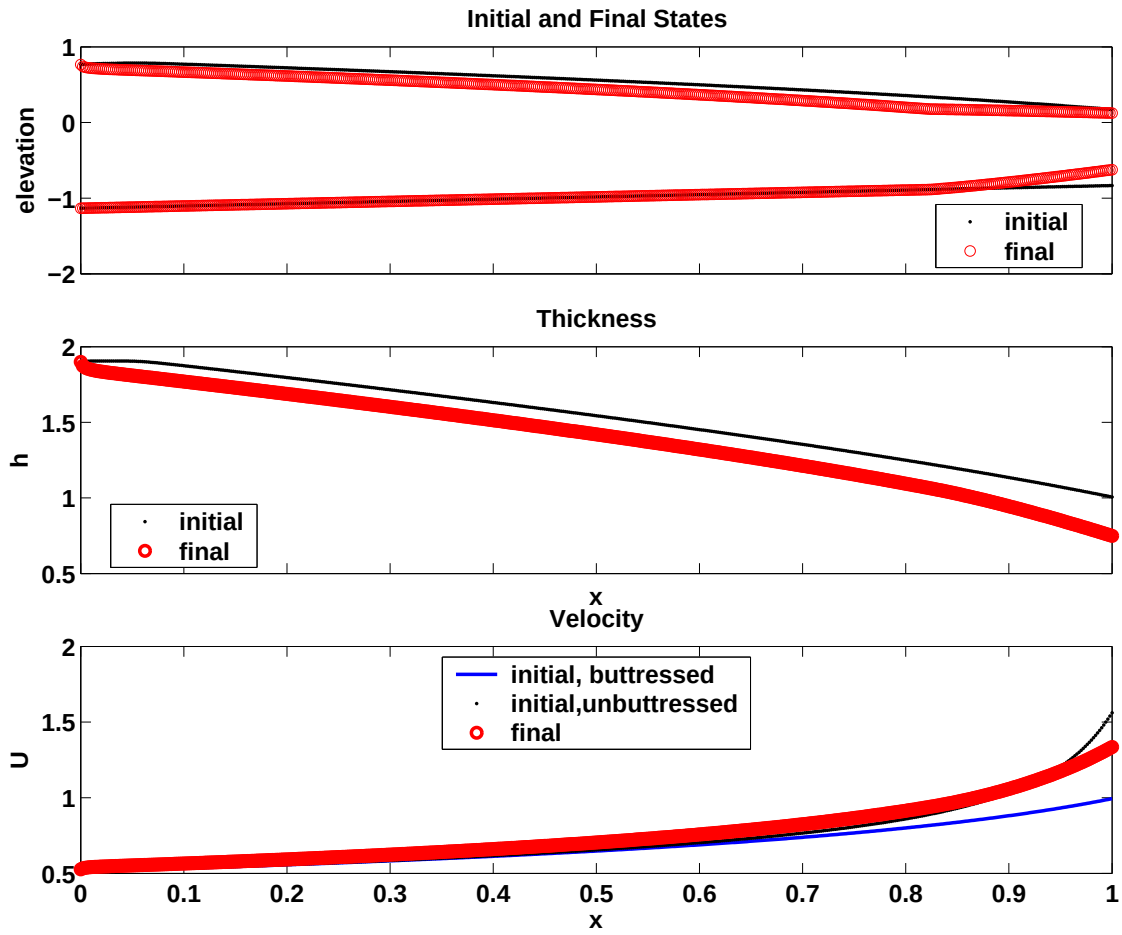

Fig. 3.2. Plot showing the initial and final states of the ice-shelf/ice-stream system for the standard or reference experiment. The upper panel shows the surface and basal elevations at the initial and final states, and the lower two panels show the initial and final thickness and velocity profiles.

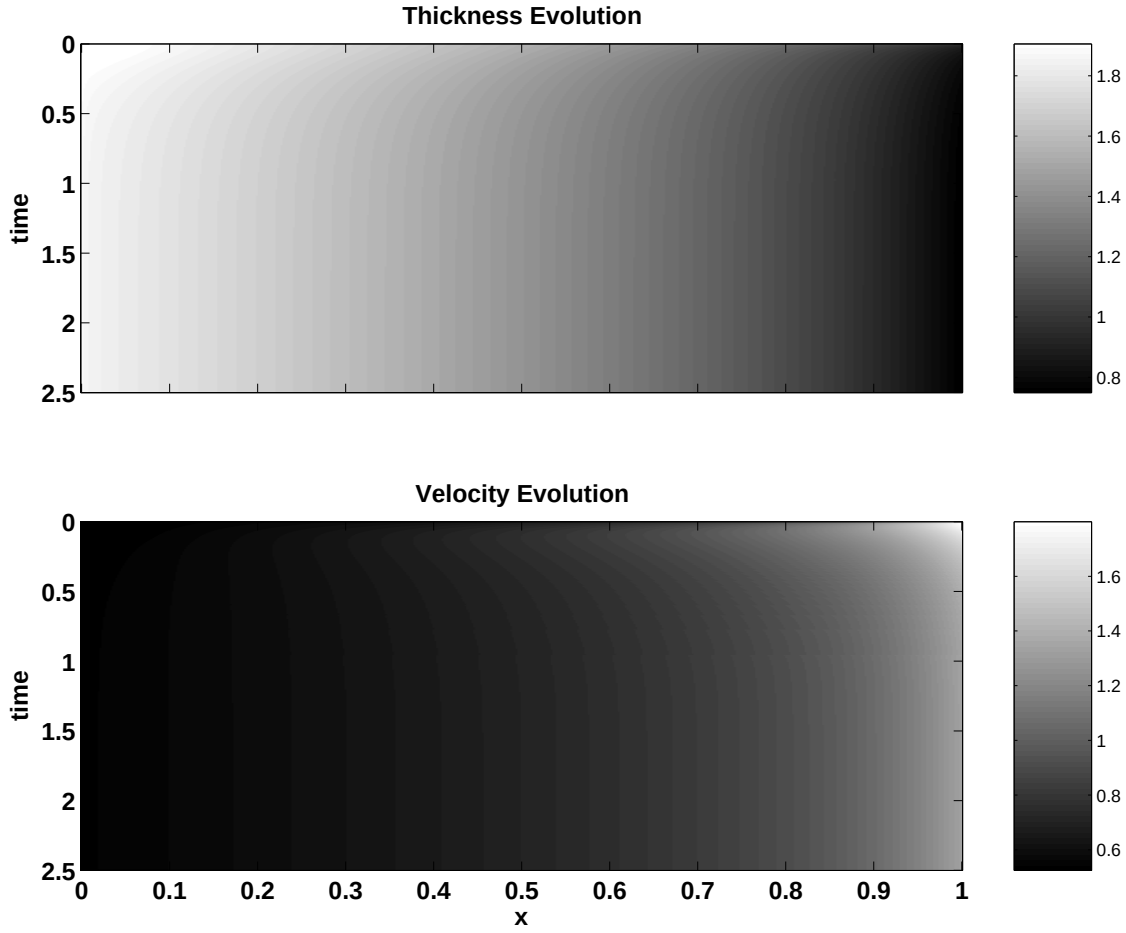

Fig. 3.3. Evolution of the thickness and velocity profiles after removal of buttressing.

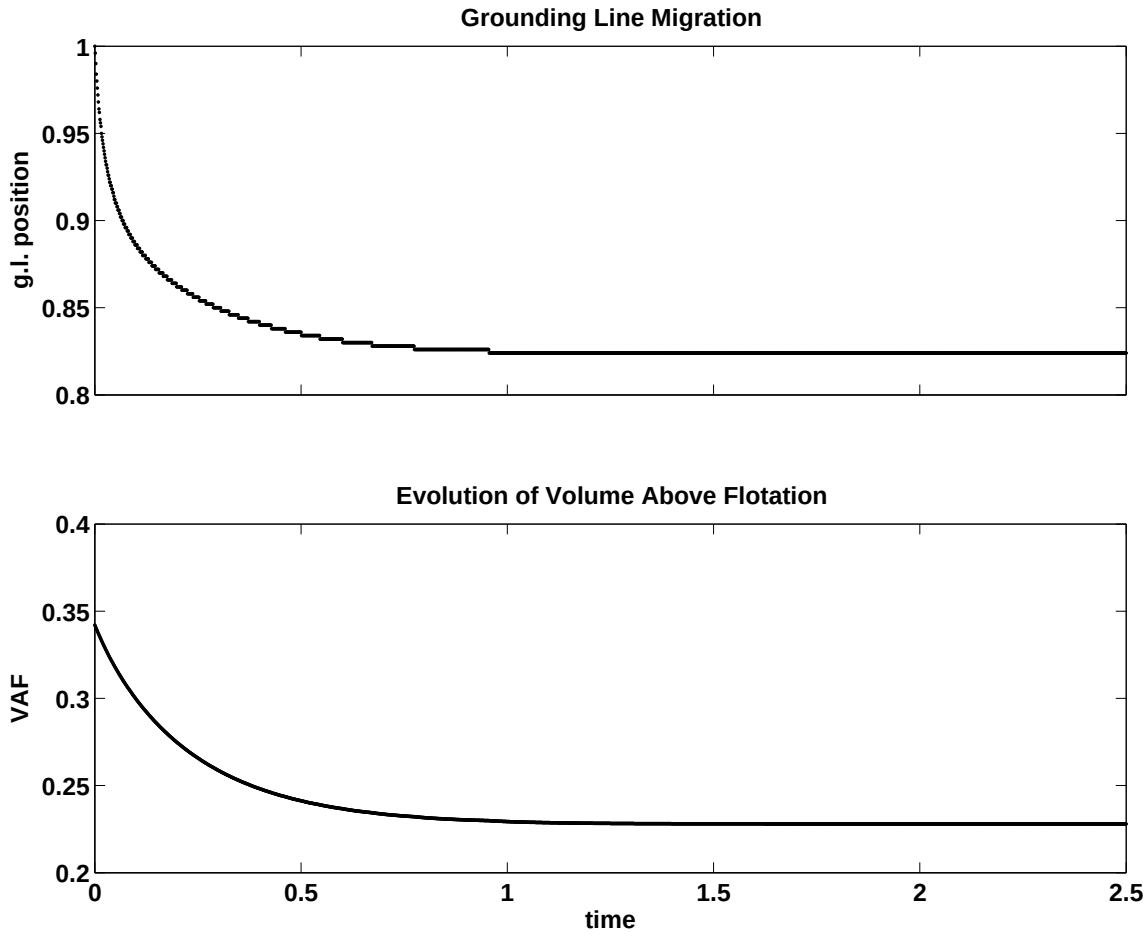

Fig. 3.4. Evolution of the grounding line (g.l.) and integrated volume above flotation (VAF) after removal of buttressing.

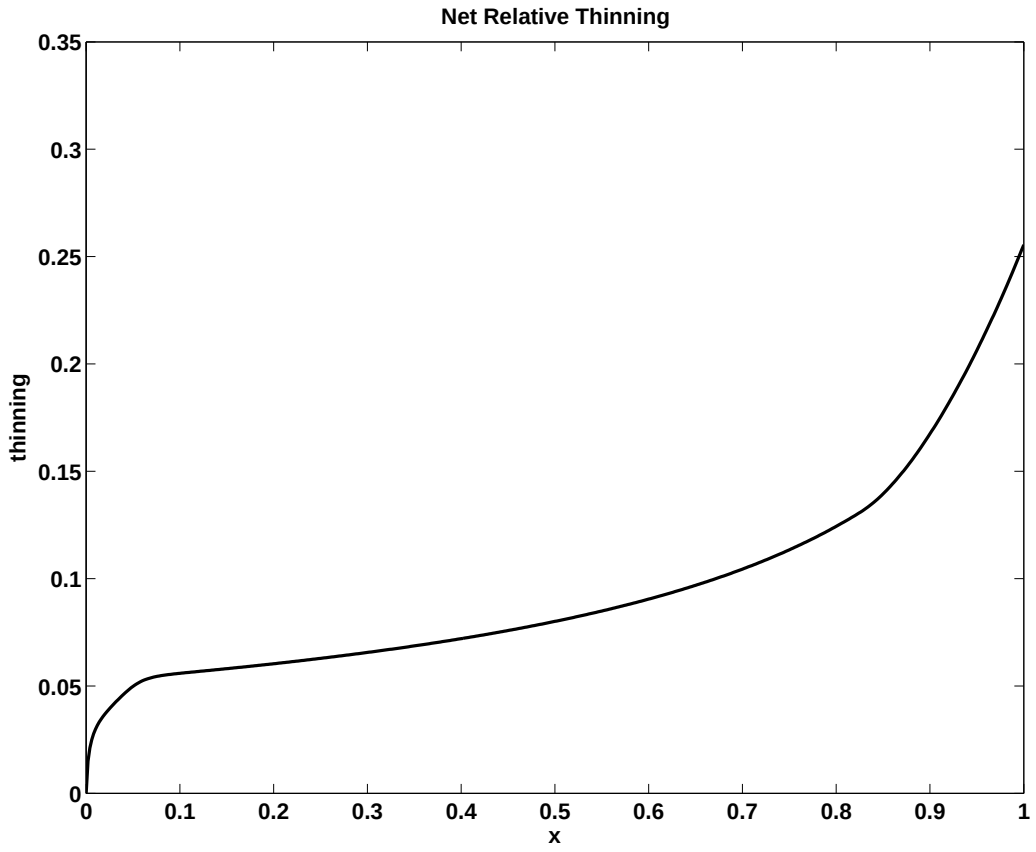

Fig. 3.5. Net relative thinning. Plot showing the distribution of relative or thickness normalized thinning. Note that thinning extends well upstream.

Table 3.2. Experiment parameter sets

experiment	G_s	β	G_b	A	h_0	u_0
reference	15	0.3	40	50	1.9	0.53
$+G_s$	18	0.3	40	50	1.9	0.53
$-\beta$	15	0.24	40	50	1.9	0.53
$+G_b$	15	0.3	48	50	1.9	0.53
$+A$	15	0.3	40	60	1.9	0.53
$-A$	15	0.3	40	40	1.9	0.53
$+h_0$	15	0.3	40	50	2.3	0.53
$+u_0$	15	0.3	40	50	1.9	0.63

Table 3.3. summary of the results of various experiments

experiment	init'l g.l.	final g.l.	g.l. retreat	init'l VAF	final VAF	VAF loss (% of init'l)
reference	1	0.82	0.18	0.34	0.23	0.11 (33%)
+20% in G_s	1	0.86	0.14	0.37	0.27	0.10 (27%)
-20% in β	1	0.83	0.17	0.35	0.24	0.11 (32%)
+20% in G_b	1	0.83	0.17	0.38	0.26	0.12 (32%)
+20% in A	0.93	0.71	0.22	0.21	0.14	0.11 (43%)
-20% in A	1	0.92	0.08	0.43	0.35	0.09 (20%)
+20% in h_0	1	0.82	0.18	0.34	0.23	0.12 (34%)
+20% in u_0	1	0.86	0.14	0.39	0.28	0.11 (28%)

Chapter 4

Conditions for the reversal of ice-stream surface slope

4.1 Introduction

A local reversal in the surface slope of an ice sheet or ice stream is of interest, both because slope reversal indicates anomalous basal conditions and because subglacial water flow is sensitive to the potential gradient provided by the ice-air surface slope.

Reversed ice-air surface slopes are observed in nature in the form of ice rumples on ice shelves [*Swithinbank*, 1986], lakes on the surface of the Greenland ice sheet and on the surface of Matanuska Glacier [*Alley et al.*, 2003b], and perhaps most importantly, on the downglacier side of Lake Vostok [*Studinger et al.*, 2003]. Ice flowing over any localized reduction in basal lubrication or any bedrock high will tend to slow, thereby reducing the magnitude of the surface slope upglacier of the obstacle or reversing that slope, and steepening the slope over the obstacle. Owing to the important role of longitudinal stresses over distances of less than a few ice thicknesses [*Budd*, 1970], there is no prohibition on local reversal of ice-air surface slope.

Here we examine the tendency to form such a slope reversal for an ice shelf grounding over a sill. We focus our efforts on the equilibrium profile of the ice flowing over a flat sill. This requires the simultaneous solution of the steady-state force and momentum balance. We next describe the model we use for this solution.

4.2 Model Description

We adopt the geometry shown in schematic form in figure (4.1) and the dimensional scales shown in table (4.1). All variables are non-dimensional unless otherwise noted. The flow is from left to right, with x being designated the along-flow coordinate direction, and with the point $x = 0$ specified as the initial grounding point.

One scale of special note is the thickness scale H. For the present study we specify that this scale correspond to the flotation thickness for a sill depth of D given the ratio r_{sw} of seawater density to ice density, such that

$$H = r_{sw} D \tag{4.1}$$

This scaling implies that where the non-dimensional thickness is greater than unity the ice is grounded, and where the thickness is less than or equal to unity the ice is afloat.

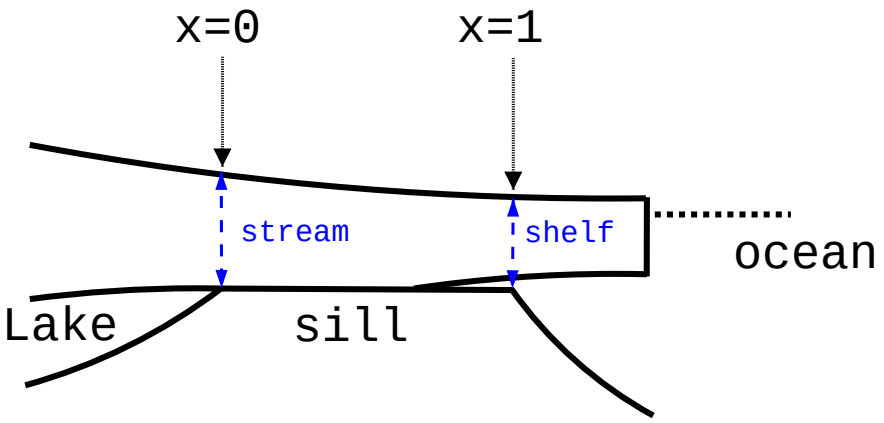

Fig. 4.1. Schematic geometry.

4.2.1 governing equations

If we neglect, primarily for the sake of simplicity, cross-flow variations in velocity and thus lateral drag, then the appropriate governing equation for the x-directed force balance is the depth-integrated Stokes equation, which in non-dimensional form is

$$\frac{\partial}{\partial x}\left(2h\nu\frac{\partial u}{\partial x}-\frac{A}{2}h^2\right) = \begin{cases} Gu^{\frac{1}{m}} & h>1 \\ -\frac{A}{2}\frac{1}{r_{sw}}\partial_x h^2 & h\leq 1 \end{cases} \qquad x\in(0,1) \tag{4.2}$$

where h is the thickness, u is the velocity, and m is the exponent for basal friction. The effective viscosity ν is defined as

$$\nu \equiv \left|\frac{\partial u}{\partial x}\right|^{\frac{1-n}{n}} \tag{4.3}$$

where $n=3$ is the flow-law exponent for ice. The non-dimensional constants A and G measure the importance to ice flow of thickness gradients and basal drag, respectively. Note that the notation from chapter (2), where the basal drag strength was labeled as G_b, has been simplified to G in the absence of any lateral drag. Similarly, the notation for the longitudinal length scale L_x has been simplified here to L. The non-dimensional numbers A and G are determined by the choice of scales and parameter values according

to the following definitions

$$A \equiv \frac{\rho_i g H}{B_i \left(\frac{U}{L}\right)^{\frac{1}{n}}} \tag{4.4}$$

$$G \equiv \frac{\tau_b L}{B_i \left(\frac{U}{L}\right)^{\frac{1}{n}} H} \tag{4.5}$$

where ρ_i is the density of ice, g is the acceleration due to gravity, $H = r_{sw} D$ is the thickness scale, B_i is the ice hardness, U is the velocity scale, L is the length scale and τ_b is the basal stress scale. Table (4.1) lists the values or range of values adopted for these scales and constants, as well as the resulting range of values for A and G.

There are two boundary conditions for the force balance. The first is that we prescribe the velocity at the inlet ($x = 0$),

$$u(0) = u_0 \tag{4.6}$$

The second boundary condition is imposed at the terminal end ($x = 1$),

$$\left[2h\nu\frac{du}{dx} - \frac{A}{2}h^2\right]_{x=1} = -f\left(\frac{A}{2}h(1)^2\right) - (1-f)\left(\frac{A}{2}\frac{1}{r_{sw}}\right)\begin{cases} 1 & h(1) > 1 \\ h(1)^2 & h(1) \leq 1 \end{cases} \tag{4.7}$$

where f is an ice-shelf buttressing parameter and $h(1)$ is the (undetermined) ice thickness at this point. Equation (4.7) is simply a linear combination of two reasonable end-members for the stress state at $x = 1$, with the weight we give each end member being determined by the value we prescribe for f. The first end member, found by imposing

$f = 0$, is the usual ice-front condition, where the difference between the depth-integrated glaciostatic and hydrostatic pressures is balanced by a tensile depth-integrated longitudinal deviatoric stress, implying a positive longitudinal strain-rate $\frac{\partial u}{\partial x}$. This is the stress state one would expect at an ice front or at the junction with a freely-floating ice shelf. The second end-member, found by setting $f = 1$, is a "fully buttressed" condition, with zero depth-integrated deviatoric stress, resulting in zero longitudinal strain-rate. The utility of f is that it allows for situations where the ice beyond $x = 1$ could be losing some momentum due to local grounding or perhaps lateral shear. In such a situation the momentum flux that must be transmitted upstream (into the modeled domain) is reduced relative to the case of a free-floating ice shelf; we model this situation by setting f to something greater than zero.

Mass balance is governed by the evolution equation

$$\partial_t h = -\partial_x (uh) \tag{4.8}$$

where t is the non-dimensional time coordinate, and we neglect any source (or sink) of mass via accumulation (ablation). Equation (4.8), which is derived from mass continuity, simply states that the time rate of change in thickness is equal to the convergence of horizontal mass flux. At the upstream boundary ($x = 0$) we prescribe the thickness

$$h(0) = h_0 \tag{4.9}$$

Given that we are interested in scenarios where the ice is at least partially grounded as it flows across the sill, and given that we have defined the thickness scale such that $h \leq 1$ implies flotation, we restrict the upstream thickness to being greater than unity,

$$h_0 > 1 \tag{4.10}$$

4.2.2 numerical model & experiments

Our goal, given values for our poorly known parameters A, G, u_0, f, and h_0, is to find out if the resulting equilibrium thickness distribution has a slope reversal. To find an equilibrium thickness distribution we start at some initial guess for the thickness and let equation (4.8) evolve toward steady-state, subject to the boundary conditions (4.6), (4.7) and (4.9) with the velocity given by equation (4.2) at each instant in the evolution. Linear finite elements are used to discretize both equation (4.2) and (4.8) in space, and equation (4.8) is discretized in time using semi-implicit finite differences (see Appendix B).

4.3 Results & Discussion

We perform 5 sets of experiments, as outlined in table (4.2). Within each set of experiments, we set the values for h_0, u_0, f and m and find equilibrium profiles for a range of A and G. For each profile we ask whether the profile has a surface slope reversal. We also ask whether the ice is grounded over the full extent of the domain, in which case we designate the profile as fully grounded.

The results for the standard experiment are shown in figure (4.2). There is clearly a transition from normal to reversed surface slope within the range of A and G chosen. The tendency is toward normal slope and partial grounding in the high-driving-stress, low-basal-drag portion of the space, and reversed slope and full grounding in the low-driving-stress-strength, high-basal-drag portion of region. Two profiles are shown in figure (4.2), as examples of the fully grounded, reversed surface-slope case and the partially grounded, normal surface-slope case. Note that the other two possible cases, that of partially grounded, reversed surface-slope and fully-grounded, normal-slope profiles, do in fact occur but occupy a smaller region of the parameter space explored.

Figures (4.3)-(4.10) show the effects of perturbations in the standard set of parameter values. It is clear that going from a linear ($m = 1$) to non-linear ($m = 12$) bed rheology makes little difference in the location of the transition in parameter space.

Decreasing the upstream thickness produces an expansion of the area of reversed surface slope for low driving stress and low basal drag. For higher driving stress and higher basal drag, decreasing the upstream thickness produces a contraction of the region of reversed surface slope. Thus, systems that are near the slope transition should be expected to seal (unseal) when low (high) in driving stress and basal drag and subjected to an upstream thinning. Similarly, upstream thinning produces an expansion of the partially-grounded region in A-G space. This is expected in the sense that as the ice thins upstream the whole of the flow must thin, which will allow ice near flotation to reach flotation and unground. This ungrounding, for high driving stress and basal drag, leads to a transition to normal slope as the area over which basal drag operates is reduced.

Increasing the upstream velocity relative to the standard case produces an expansion of the reversed surface-slope and fully grounded regions of A-G. This is expected because higher velocity makes the profile becomes more advection-dominated. Similarly, introducing buttressing expands the reversed surface-slope and fully-grounded regions. This follows from a weakening of the stretching required within the ice as buttressing is introduced at the downstream end.

4.4 Conclusions

From our exploration of parameter space, we see that the reversed surface-slope region invariably occupies the lower A, higher G portion of parameter space. Because these parameters are, respectively, directly and inversely proportional to the thickness scale, we see that thinning tends toward slope reversal. Similarly, making the bed stickier, as measured by G, tends toward slope-reversal. Conversely, decreasing buttressing tends toward normal slopes. Thus we see that a transition to slope reversal is favored by thinning, strengthening the bed, and increasing ice-shelf buttressing.

Given that the parameter values used in this study are well within reasonable glaciological values, we can say with confidence that we should expect slope-reversals. To the extent that these slope-reversals aid in trapping water within subglacial lakes, we can say that these results are at least consistent with outburst flooding, as described by *Alley et al.* [2003a].

Variable	Scale	Value or range of scale assumed here
h	$H = r_{sw}D$	$1.12 * (1 - 5 \times 10^2)$ m
x	L	$3 \times 10^3 - 3 \times 10^4$ m
u	U	$2 - 6 \times 10^{-5}$ ms^{-1}
t	L/U	$5 - 150 \times 10^7$ s
B_i	B_i	$1 - 2 \times 10^8$ Pa s$^{1/3}$
τ_b	τ_b	$5 \times 10^3 - 2 \times 10^5$ Pa
A	$\frac{\rho_i g r_{sw} D L^{1/3}}{B_i U^{\frac{1}{3}}}$	$2 - 60$
G	$\frac{\tau_b L^{4/3}}{r_{sw} D B_i U^{1/3}}$	$5 \times 10^{-2} - 6 \times 10^2$

Table 4.1. Scales used to non-dimensionalize the force and mass balance equations along with their boundary conditions.

experiment	A	G	h_0	u_0	f	m
standard	2-30	0.1-6	1.1	1	0	1
$+h_0$	2-30	0.1-6	1.01	1	0	1
$+u_0$	2-30	0.1-6	1.1	1.5	0	1
$+f$	2-30	0.1-6	1.1	1	0.5	1
$+m$	2-30	0.1-6	1.1	1	0	12

Table 4.2. Sets of parameter values for the various numerical experiments

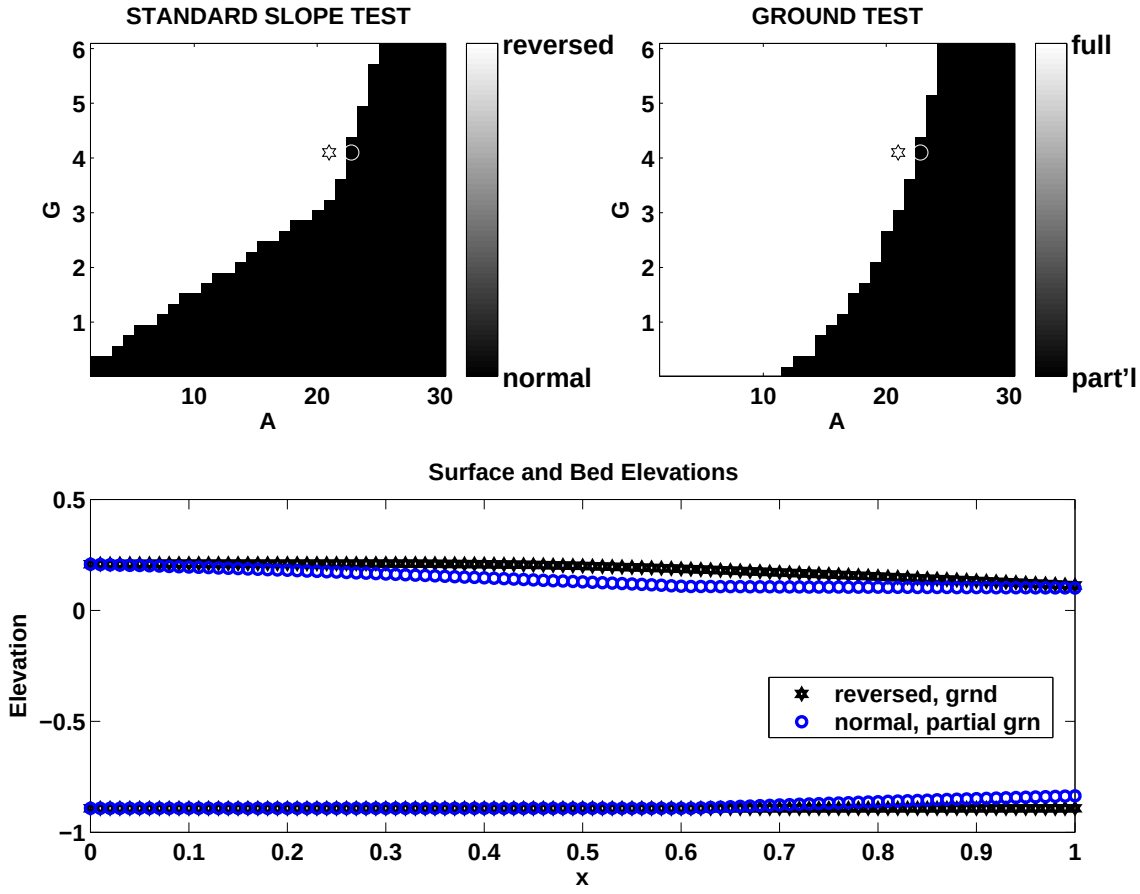

Fig. 4.2. Results of the standard experiment. The upper left panel shows the transition from normal to reversed surface slope in A-G space. The upper right panel shows the transition from fully to partially grounded ice in the same space. The lower panel shows the equilibrium surface and bed profiles for the two points in A-G space marked on the upper panels, chosen to exemplify profiles on either side of the transitions.

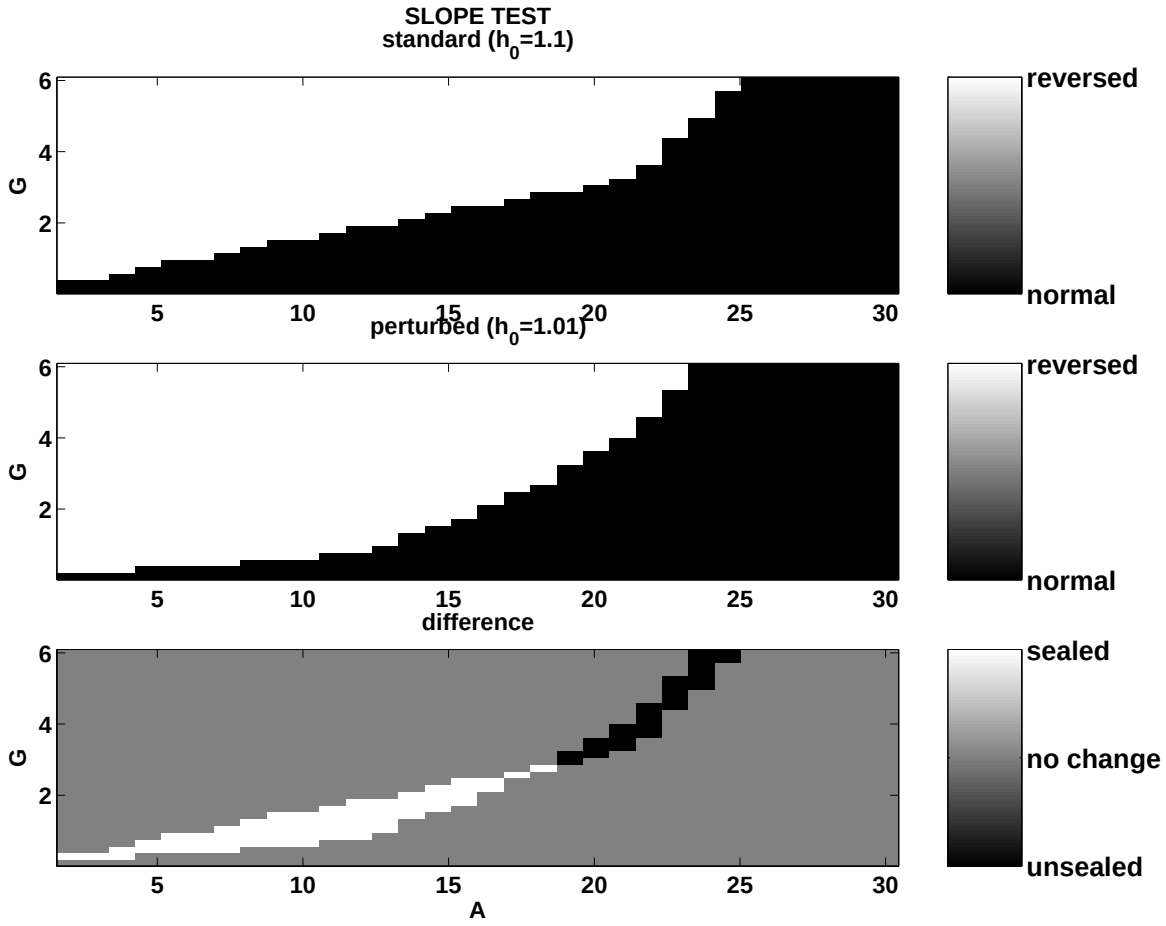

Fig. 4.3. Effect of h_0 perturbation in slope transition. The upper panel shows the transition from normal to reversed surface slope for the standard experiment. The middle panel shows this transition for a smaller value of the upstream thickness h_0. The lower panel shows the difference between the two cases and indicates how a change in the upstream thickness might seal (normal goes to reversed slope) or unseal (reversed slope goes to normal) the system.

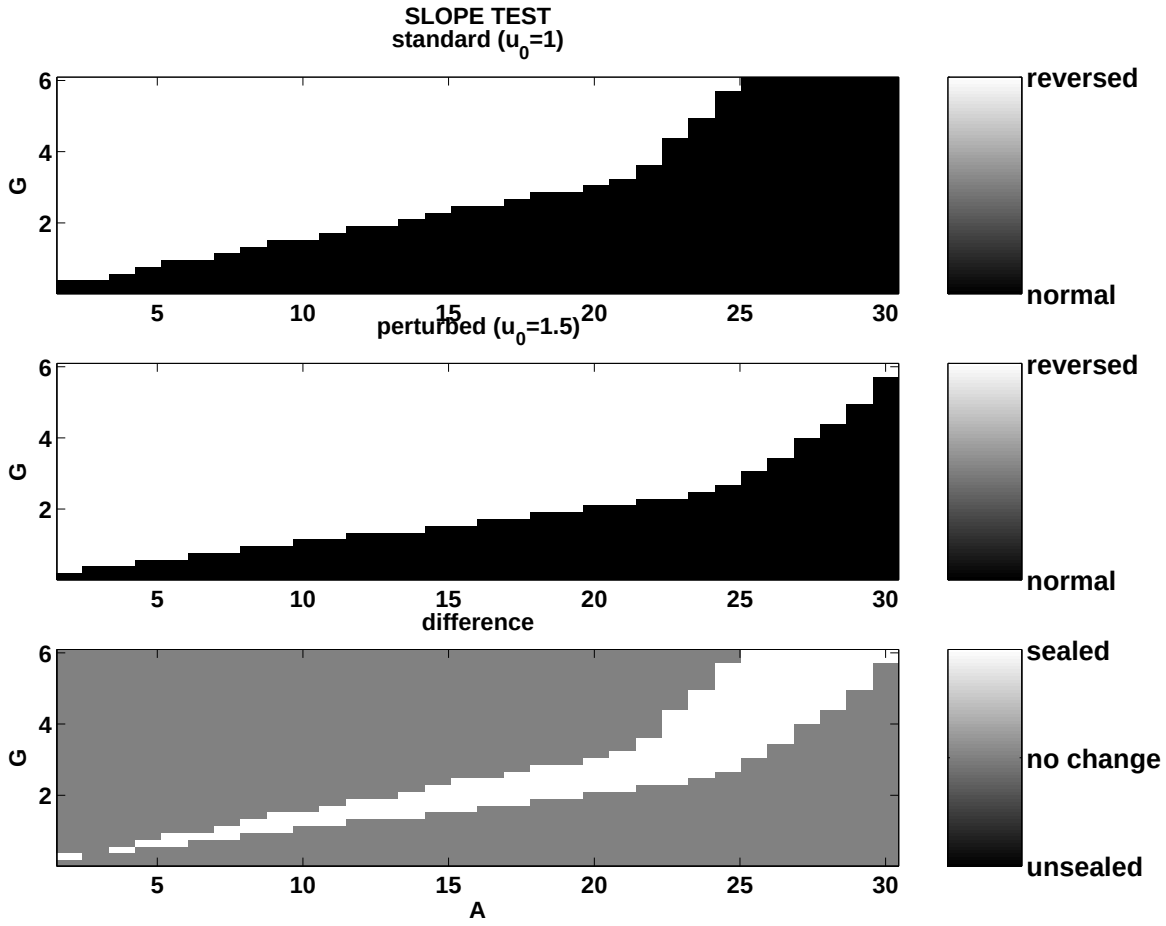

Fig. 4.4. Effect of u_0 perturbation in slope transition. The upper panel shows the transition from normal to reversed surface slope for the standard experiment. The middle panel shows this transition for a smaller value of the upstream velocity u_0. The lower panel shows the difference between the two cases and indicates how a change in the upstream velocity might seal (normal goes to reversed slope) or unseal (reversed slope goes to normal) the system.

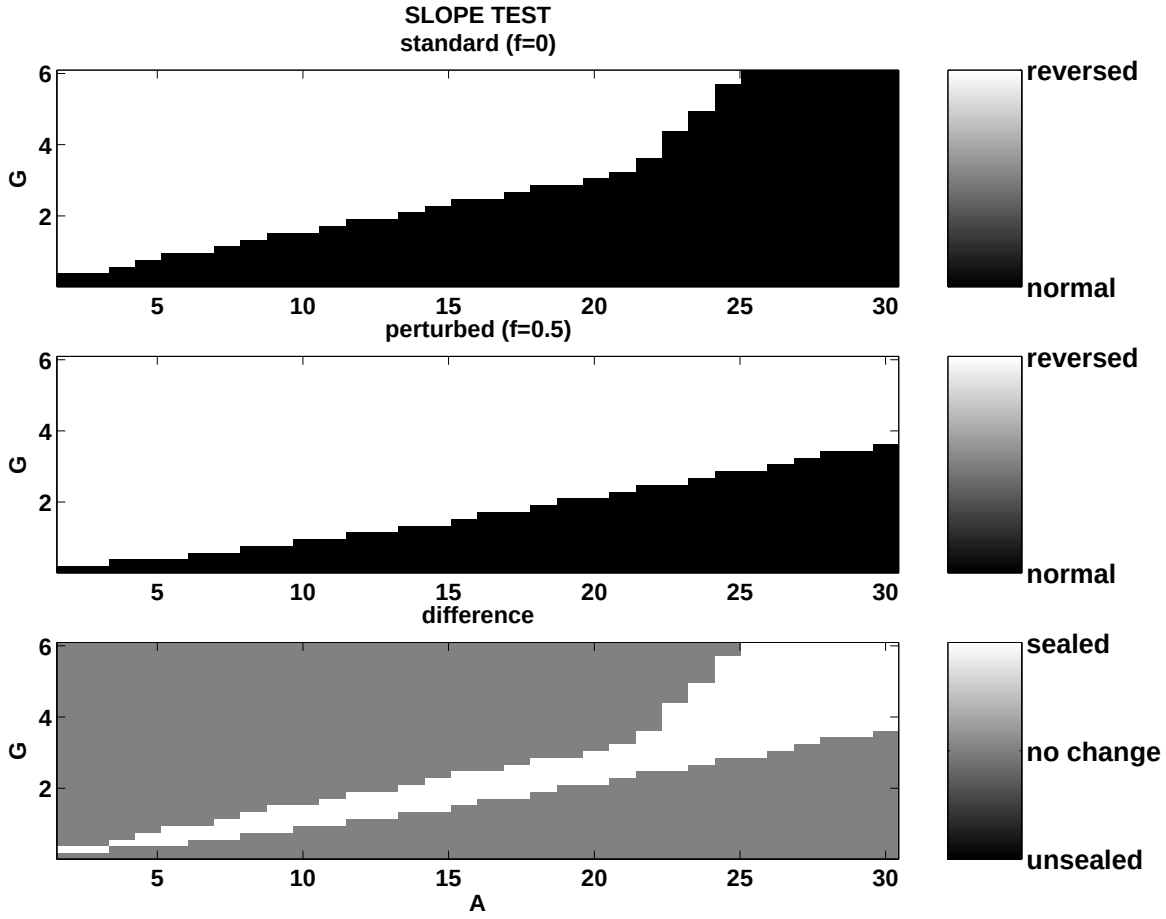

Fig. 4.5. Effect of f perturbation in slope transition. The upper panel shows the transition from normal to reversed surface slope for the standard experiment. The middle panel shows this transition for an increase in buttressing. The lower panel shows the difference between the two cases and indicates how a change in buttressing might seal (normal goes to reversed slope) or unseal (reversed slope goes to normal) the system.

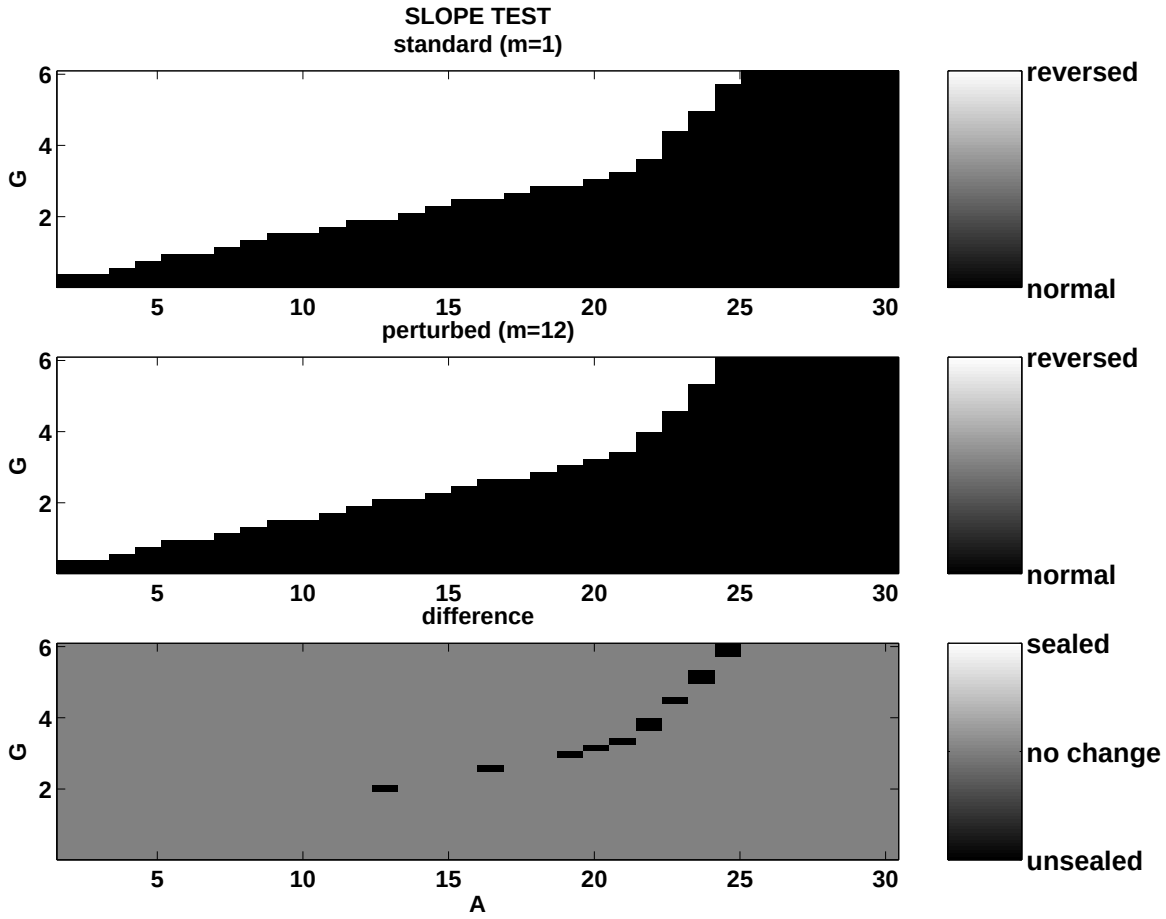

Fig. 4.6. Effect of m perturbation in slope transition. The upper panel shows the transition from normal to reversed surface slope for the standard experiment, where the bed exponent m is set to unity. The middle panel shows this transition for a non-linear ($m = 12$) bed exponent. The lower panel shows the difference between the two cases and indicates how the character of the bed rheology might affect the character of the transition.

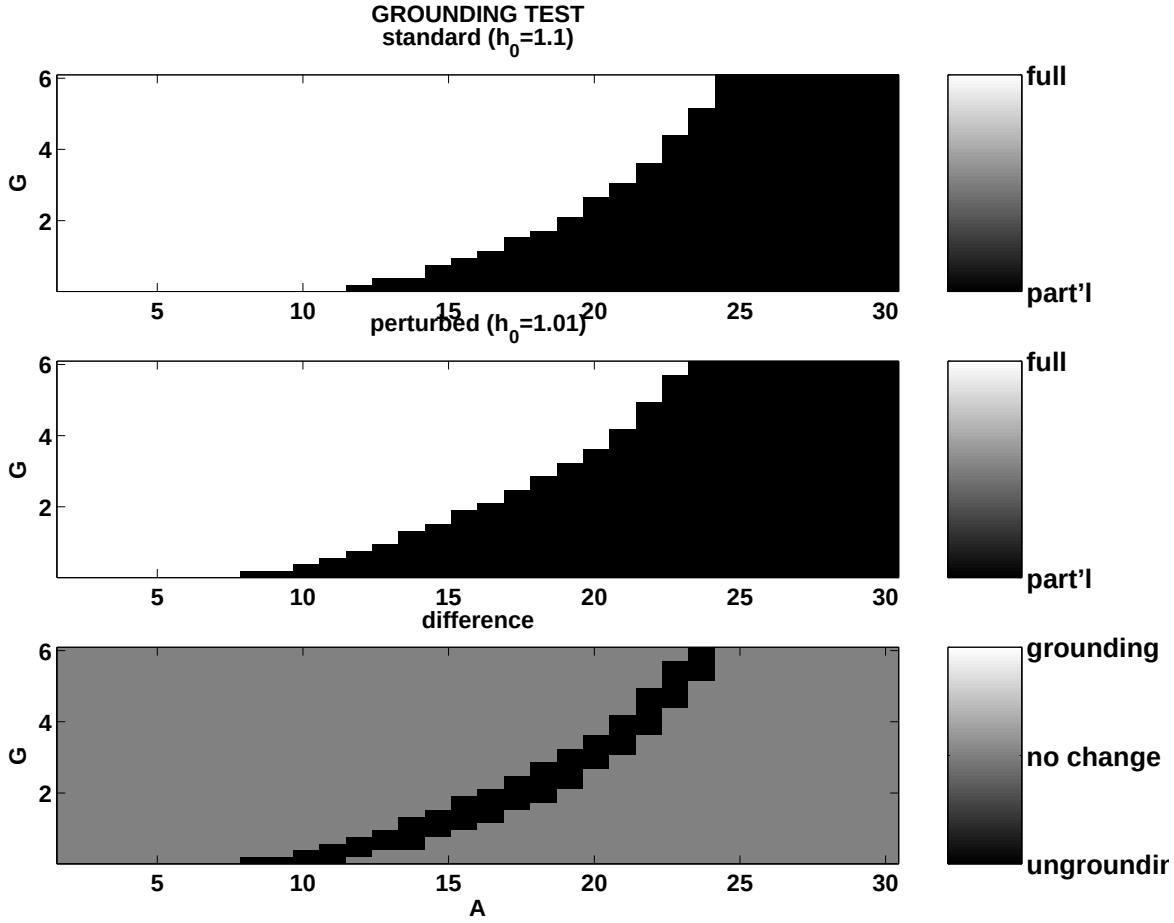

Fig. 4.7. Effect of h_0 perturbation in grounding transition. The upper panel shows the transition from fully to partially grounded ice for the standard experiment. The middle panel shows this transition for a smaller value of the upstream thickness h_0. The lower panel shows the difference between the two cases and indicates how a change in the upstream thickness might ground or unground the system.

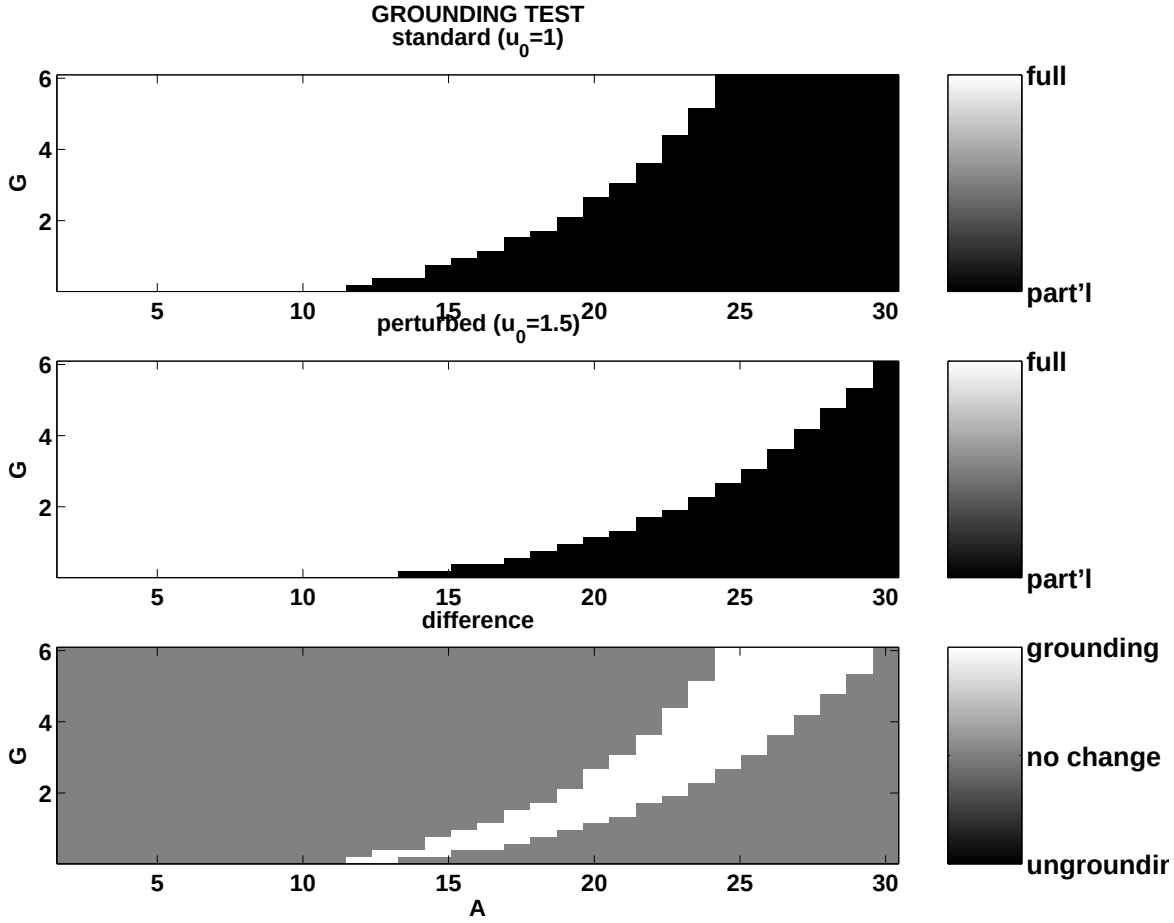

Fig. 4.8. Effect of u_0 perturbation in grounding transition. The upper panel shows the transition from fully to partially grounded ice for the standard experiment. The middle panel shows this transition for a larger value of the upstream velocity u_0. The lower panel shows the difference between the two cases and indicates how a change in the upstream velocity might ground or unground the system.

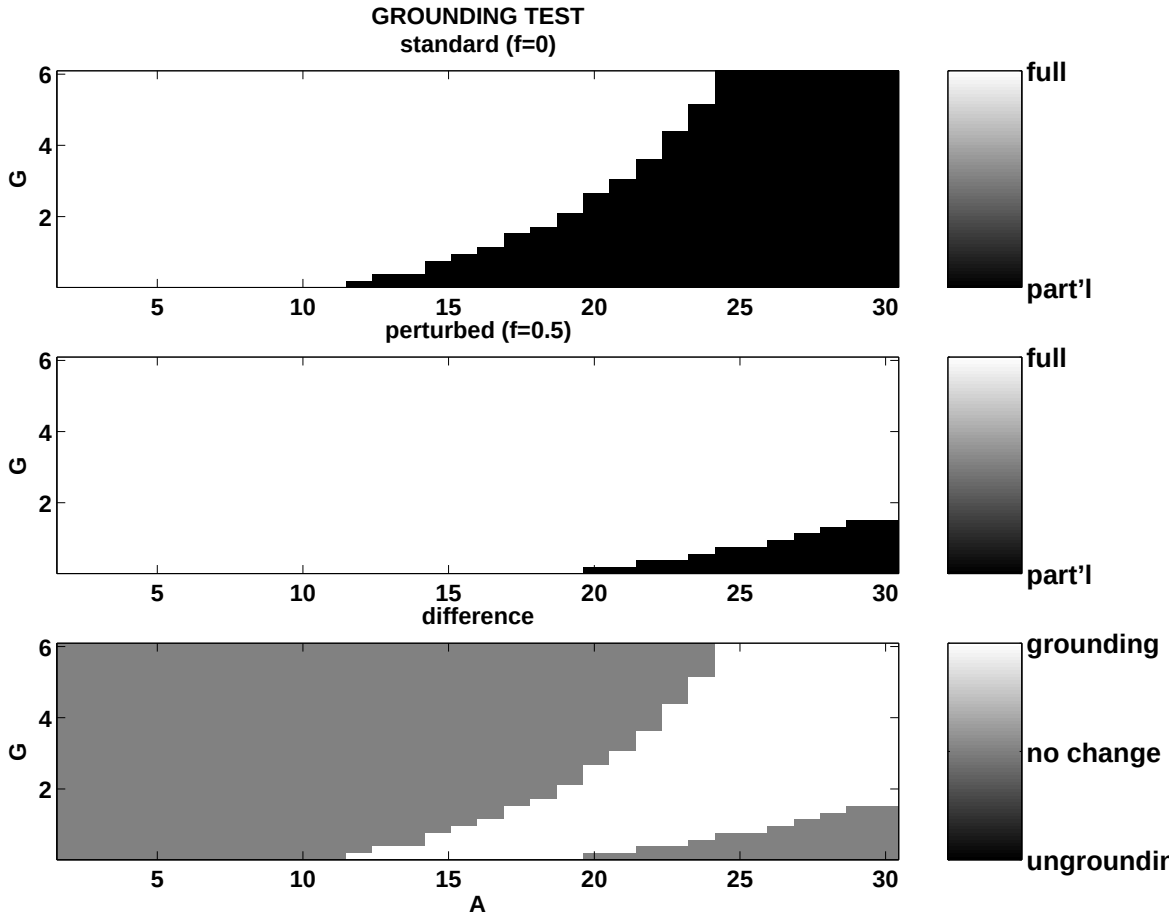

Fig. 4.9. Effect of f perturbation in grounding transition. The upper panel shows the transition from fully to partially grounded ice for the standard experiment. The middle panel shows this transition for an increase in buttressing. The lower panel shows the difference between the two cases and indicates how a change in buttressing might ground or unground the system.

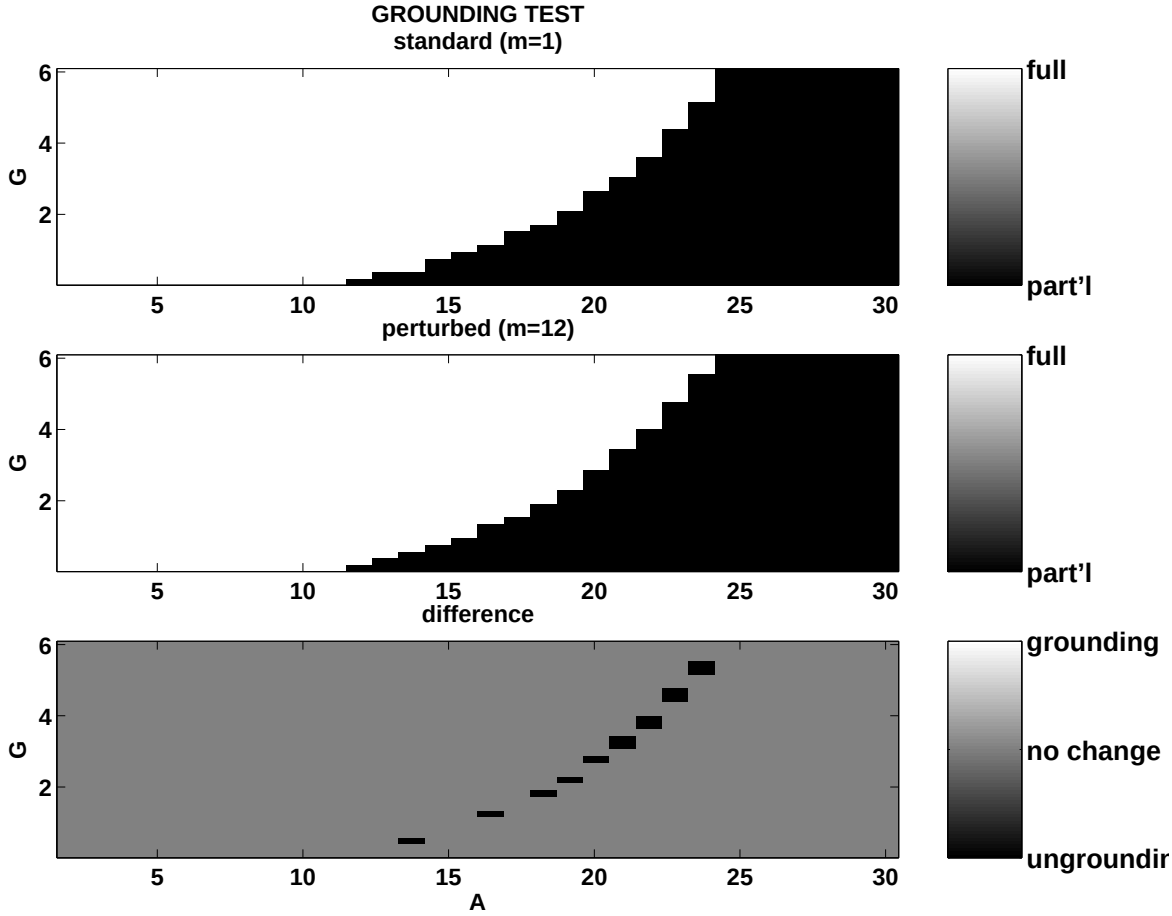

Fig. 4.10. Effect of m perturbation in grounding transition. The upper panel shows the transition from fully to partially grounded ice for the standard experiment. The middle panel shows this transition for a non-linear value for the bed exponent m. The lower panel shows the difference between the two cases and indicates how the character of the bed rheology might affect the character of the transition.

Appendix A

Notation

variable const. or param.	description	units when dimensional
A	driving stress strength	
B_i	ice hardness	Pa $\mathrm{s}^{\frac{1}{n}}$
B_b	basal material hardness	Pa $\mathrm{s}^{\frac{1}{m}}$
B_s	lateral ice hardness	Pa $\mathrm{s}^{\frac{1}{n}}$
β	channel bed slope	
D	sill depth	m
$\delta_y U$	scale for lat. change in u	m s^{-1}
$\delta_z U$	scale for vert. change in u	m s^{-1}
$\delta_x V$	scale for long. change in v	m s^{-1}
$\delta_y V$	scale for lat. change in v	m s^{-1}
$\delta_z V$	scale for vert. change in v	m s^{-1}
$\delta_x W$	scale for long. change in w	m s^{-1}
$\delta_y W$	scale for lat. change in w	m s^{-1} b
$\underline{\dot{\epsilon}}$	strain rate tensor	s^{-1}

variable, const., or param.	description	units when dimensional
$\dot{\epsilon}_{ij}$	strain rate components	s^{-1}
f	buttressing param.	
G	basal drag strength (Ch 4)	
G_b	basal drag strength	
G_s	side drag strength	
$g = (9.81)$	gravitation acceleration	$\mathrm{m\ s}^{-2}$
H	thickness scale	m
$h(x)$	thickness	m
h_b	basal bound. layer thickness	m
h_f	flotation thickness	m
h_0	upstream thickness	m
L_x	along-flow length scale	m
L_y	cross-flow length scale	m
m	basal flow-law exponent	
$n = 3$	ice flow-law exponent	
ν	viscosity	Pa s
p	pressure	Pa
r_{sw}	nondim. seawater density	
$\rho_i (= 917)$	density of ice	$\mathrm{kg\ m}^{-3}$
$\rho_{sw} (= 1028)$	density of seawater	$\mathrm{kg\ m}^{-3}$
T	time scale	s

variable, const. or param.	description	units when dimensional
t	time	s
τ_b	dynamic basal drag	Pa
τ_y	dynamic lateral drag	Pa
τ_{ij}	stress components	Pa
τ'_{ij}	deviatoric stress components	Pa
U	along-flow velocity scale	m s^{-1}
u	along-flow velocity component	m s^{-1}
u_0	upstream velocity	m s^{-1}
v	cross-flow velocity component	m s^{-1}
w	vertical velocity component	m s^{-1}
x	along-flow coordinate	m
y	cross-flow coordinate	m
y_s	width of lateral bound. layer	m
z	vertical coordinate	m
$z_b(x)$	basal elevation	m
$z_r(x)$	channel bed elevation	m
$z_s(x)$	surface elevation	m
$\langle\rangle_z$	vertical averaging operator	
$\langle\rangle_y$	lateral averaging operator	
∂_x	longitudinal derivative	m^{-1}
∂_y	lateral derivative	m^{-1}
∂_z	vertical derivative	m^{-1}

Appendix B

Numerical model of ice-stream/ice-shelf evolution equation

B.1 Introduction

The purpose of this appendix is to set out the numerical details used in the prognostic mass-balance component model applied in this thesis. As in chapters (3) and (4), our variables are non-dimensional. The goal is to capture the evolution in thickness $h = h(x,t)$ governed by the continuity-derived evolution equation

$$\partial_t h = -\partial_x (uh), \quad 0 < x \leq 1, \quad 0 < t \leq t_{final} \tag{B.1}$$

where x and t are the spatial and temporal coordinates, $h = h(x,t)$ is the ice thickness, $u = u(x,t)$ is the depth averaged x-directed velocity, and t_{final} is the final time. Note that we have neglected accumulation. At the upstream end ($x = 0$), the thickness is prescribed

$$h(0,t) = h_0, \quad 0 \leq t \leq t_{final} \tag{B.2}$$

At the downstream end ($x = 1$) we prescribe neither thickness nor flux, allowing whatever volume of material to freely pass out of the domain. The initial condition is prescribed as

$$h(x,0) = h_{start}(x), \quad 0 < x \leq 1 \tag{B.3}$$

The development of a numerical model of the problem defined in equations (B.1), (B.2) and (B.3) involves two main steps, (i) spatial discretization, and (ii) temporal discretization. Spatial discretization produces a system of ordinary differential equations for the values on the spatial nodes of the thickness through time. This system of ordinary differential equations is sometimes referred to as the semidiscrete form of the model problem [e.g., *Becker et al.*, 1981, p. 250]. Temporal discretization, as implemented here, involves incrementally integrating the semidiscrete form forward in time.

B.2 Spatial Discretization

A variant of the finite element method is used to create the semidiscrete form. The procedure is very similar to that in *Becker et al.* [1981, p.246-250], but for brevity I drop even their rather informal mathematical formality.

We begin by writing equation (B.1) in weighted residual form

$$\int_{\Omega} w \left\{ \partial_t h + \partial_x \left(uh \right) \right\} dx = 0 \tag{B.4}$$

We now partition the domain $0 = x_1 < x_2 < \ldots < x_N = 1$ where N is the total number of nodes.

The interpolated approximation of w on the interval $\Omega = \{0 < x < 1\}$ is defined as

$$w(\Omega) \equiv \left(\vec{\varphi} + \gamma \partial_x \left(\vec{\varphi} \right) \right) \cdot \vec{w} \tag{B.5}$$

where $\vec{w}$ is the vector of nodal values of w, γ is an upwind-weighting parameter, and $\vec{\phi}$ a vector of piece-wise linear interpolation functions, defined such that $\phi_1(x_1) = 0$ and

$$\varphi_i(x_j) = \begin{cases} 1, & i = j \\ 0, & i \neq j \end{cases} \qquad i, j = 2, \ldots, N \tag{B.6}$$

Substituting the definition (B.5) into the weighted residual form (B.4) yields

$$\begin{aligned} \vec{w}^T \cdot \int_\Omega \left(\vec{\varphi}^T + \gamma \partial_x \vec{\varphi}^T\right) \partial_t h dx &= \vec{w}^T \cdot \Big[\int_\Omega \left\{ \left(\partial_x \vec{\varphi}^T\right) uh - \gamma \left(\partial_x \vec{\varphi}^T\right) \partial_x (uh) \right\} dx \\ &\quad - (\varphi uh)_{x=1} \Big] \end{aligned} \tag{B.7}$$

Given our earlier partition, the interval Ω may be decomposed into a finite set of subdomains Ω_e such that

$$\sum_e^{N_{el}} \int_{\Omega_e} dx = \int_\Omega dx \tag{B.8}$$

Define the 1x2 vector of elemental shape functions as the subset of $\vec{\varphi}$ that is non-trivial within the element Ω_e,

$$\begin{aligned} \vec{\Psi}(\Omega_e) &\equiv \vec{\varphi}(\Omega_e) \\ &= \begin{bmatrix} \frac{x_2 - x}{\delta x} & \frac{x - x_1}{\delta x} \end{bmatrix} \\ &= \begin{bmatrix} 1 - \lambda & \lambda \end{bmatrix} \end{aligned} \tag{B.9}$$

where $\lambda \equiv \frac{x - x_1}{\delta x}$ and $\delta x = x_2 - x_1$.

Let the u, h and $\partial_t h$ be interpolated on each interval using (B.9) such that

$$u(\Omega_e) = \vec{\Psi} \cdot \vec{u}_e \tag{B.10}$$

$$h(\Omega_e) = \vec{\Psi} \cdot \vec{h}_e \tag{B.11}$$

$$\partial_t h(\Omega_e) = \vec{\Psi} \cdot \vec{\partial_t h}_e \tag{B.12}$$

where $\vec{u}_e$, $\vec{h}_e$ and $\vec{\partial_t h}_e$ are the nodal values of velocity, thickness, and time-rate-of-change of thickness for the e^{th} element. We will treat the upwinding parameter γ as an elemental quantity, such that

$$\gamma(\Omega_e) = \gamma_e \tag{B.13}$$

Substituting the local or elemental approximations (B.10)-(B.13) into the weighted residual form (B.7) and looking at the individual terms, we have

$$\vec{w}_e^T \cdot \int_{\Omega_e} \left(\partial_x \vec{\Psi}^T u h \right) dx = \vec{w}_e^T \cdot \frac{1}{6} \begin{bmatrix} -(2u_1 + u_2) & -(u_1 + 2u_2) \\ (2u_1 + u_2) & (u_1 + 2u_2) \end{bmatrix} \cdot \vec{h}_e$$

$$-\vec{w}_e^T \cdot \int_{\Omega_e} \gamma \left(\partial_x \vec{\Psi}^T \right) \partial_x (uh) \, dx = \vec{w}_e^T \cdot \frac{\gamma_e}{\delta x} \begin{bmatrix} -u_1 & u_2 \\ u_1 & -u_2 \end{bmatrix} \cdot \vec{h}_e$$

$$\vec{w}_e^T \cdot \int_{\Omega_e} \vec{\Psi}^T \partial_t h dx = \vec{w}_e^T \cdot \frac{\delta x}{6} \begin{bmatrix} 2 & 1 \\ 1 & 2 \end{bmatrix} \cdot \vec{\partial_t h}_e$$

$$\vec{w}_e^T \cdot \int_{\Omega_e} \gamma \partial_x \vec{\Psi}^T \partial_t h dx = \vec{w}_e^T \cdot \frac{\gamma_e}{2} \begin{bmatrix} -1 & -1 \\ 1 & 1 \end{bmatrix} \cdot \vec{\partial_t h}_e$$

where u_1 and u_2 are the nodal values of velocity on the given element.

Given these terms, the weighted residual form (B.7) may be expressed

$$\sum_e \vec{w}_e^T \cdot \mathbf{M}_e \cdot \vec{\partial_t h}_e = \sum_e \vec{w}_e^T \cdot \mathbf{F}_e \cdot \vec{h}_e - \vec{w} \cdot (\varphi u h)_{x=1} \tag{B.14}$$

where

$$\mathbf{M}_e \equiv \frac{\delta x}{6} \begin{bmatrix} 2 & 1 \\ 1 & 2 \end{bmatrix} + \frac{\gamma_e}{2} \begin{bmatrix} -1 & -1 \\ 1 & 1 \end{bmatrix} \tag{B.15}$$

$$\mathbf{F}_e \equiv \frac{1}{6} \begin{bmatrix} -(2u_1 + u_2) & -(u_1 + 2u_2) \\ (2u_1 + u_2) & (u_1 + 2u_2) \end{bmatrix} + \frac{\gamma_e}{\delta x} \begin{bmatrix} -u_1 & u_2 \\ u_1 & -u_2 \end{bmatrix} \tag{B.16}$$

The matrices $\mathbf{M}_e$ and $\mathbf{F}_e$ are the elemental or local mass and flux matrices, respectively.

In terms of the global rather than elemental vectors of nodal values, equation (B.14) becomes

$$\vec{w}^T \cdot \mathbf{M} \cdot \vec{\partial_t h} = \cdot w^T \mathbf{F}(\vec{u}) \cdot \vec{h} \tag{B.17}$$

where $\mathbf{M}$ and $\mathbf{F}$ are the global mass and flux (or capacitance and stiffness) matrices assembled from the local matrices defined in equations (B.15) and (B.16). As is standard in finite element methods, the arbitrary nature of the test function begets, through linear independence [e.g., *Becker et al.*, 1981, p. 13], the requirement that the following matrix equation must be satisfied

$$\mathbf{M} \cdot \vec{\partial_t h} = \mathbf{F}(\vec{u}) \cdot \vec{h} \tag{B.18}$$

Equation (B.18) is a semidiscrete form of equation (B.1). It differs from what one might call a 'standard Galerkin' semidiscrete form because the interpolation of the test function is different, by virtue of the upwinding term in equation (B.5), from that for the other variables and in particular from the linear interpolation of both time-rate of change in thickness and the thickness. For non-zero γ this is a so-called 'Petrov-Galerkin' formulation. We adopt an upwinded Petrov-Galerkin formulation here because of the purely advective nature of the evolution equation (B.1). In effect the upwind weighting biases the discretization in the upwind direction, mimicking the natural bias of advective systems. This aids in both stability and accuracy.

B.3 Time Discretization

The semidiscrete form (B.18) is a system of first-order ordinary differential equations (ODEs) in the nodal thickness values $\vec{h} = \vec{h}(t)$ [1]. To integrate this system forward in time, we adopt fully backward or fully implicit [in the sense of *Press et al.*, 1992, p. 848] differencing in time

$$\frac{\delta \vec{h}}{\delta t} = \partial_t \vec{h}(t + \delta t) \tag{B.19}$$

With this differencing equation (B.18) is approximated

$$\mathbf{M} \cdot \delta \vec{h} = \delta t \mathbf{F} \left(\vec{u}(t + \delta t) \right) \cdot \left(\vec{h} + \delta \vec{h} \right)$$

[1] One might think that a solution for these values through time is now as close as a standard canned ODE solver. That would be wrong, at least for ice-stream/ice-shelf problems, because the non-local nature of the flux (the velocity depends on the thickness field, not just the local thickness), which feeds into the right-hand side of (B.18), makes the semidiscrete form very numerically stiff [e.g., *Strang*, 1986, p. 570].

Rearranged, this forms

$$\left((\delta t)^{-1} \mathbf{M} - \mathbf{F}\left(\vec{u}(t+\delta t)\right) \right) \cdot \delta\vec{h} = \mathbf{F}\left(\vec{u}(t+\delta t)\right) \cdot \vec{h} \tag{B.20}$$

It is this matrix problem that is solved, given nodal thicknesses $\vec{h}(t)$ at time t, for $\delta\vec{h}$ and thus the nodal thicknesses $\vec{h}(t+\delta t) = \vec{h}(t)+\delta\vec{h}$ at time $t+\delta t$. Because the matrices on the left- and right-hand side are both dependent on the future thickness, through the future velocity $u(t+\delta t)$, this matrix problem must be iterated to convergence.

B.4 Summary

The model problem has now become one of solving for the nodal thickness array at a discrete series of points in time given an initial thickness array and equation (B.20). Implicit in this process is that the model couples to a velocity model that returns the appropriate velocity for a given thickness array. Given such a model, and the algorithm outlined here, implementation is a simple matter of coding in one's favorite programming language, preferably one with efficient matrix handling capability such as Matlab®.

The approach used here is very similar to that used by *MacAyeal and Lange* [1988] and more recently by *Hulbe* [1998], which both employed backward differencing in time. The only real difference between the method outlined here and that of the aforementioned authors is the use here of a true[2] Petrov-Galerkin or upwinded finite element spatial discretization. A careful literature seach suggests that the present work may be the first

[2]Some in glaciology have used upwind-biased artifical diffusion methods that they referred to as Petrov-Galerkin [e.g., *MacAyeal*, 1997, p. 287], but because these approaches only introduce a extra, diffusion-like, term, and do not employ a different weighting scheme for the test and trial functions, they are not formally Petrov-Galerkin.

documented use of such an upwind Petrov-Galerkin algorithm for glaciological purposes. As mentioned in section (B.3) this type of formulation aids in stability, accuracy, and ultimately improved computational efficiency. While not shown here, tests run using this formulation for the case of the constant advection of a step function in thickness showed good agreement with the analytic solution, and an improved damping of numerical errors in the vicinity of the step, when compared to the standard ($\gamma = 0$) Galerkin approach.

Bibliography

Alley, R. B., 1991. Deforming-bed origin for southern Laurentide till sheets. Journal of Glaciology, 37: 67–76.

Alley, R. B. and Bindschadler, R. A., 2001. The West Antarctic Ice Sheet and Sea-Level Change. In: Alley, R. B. and Bindschadler, R. A. (Editors), The West Antarctic Ice Sheet: Behavior and Environment. Vol. 77 of Antarctic Research Series. pp. 1–11. American Geophysical Union, Washington, D.C.

Alley, R. B. and Whillans, I. M., 1984. Response of the East Antarctic ice sheet to sea-level rise. Journal of Geophysical Research, 89c: 6487–6493.

Alley, R. B., Blankenship, D. D., Bentley, C. R. and Rooney, S. T., 1986. Deformation of till beneath Ice Stream B, West Antarctica. Nature, 322: 57–59.

Alley, R. B., Dupont, T. K., Parizek, B. R., Anandakrishnan, S., Lawson, D. E., Larson, G. J. and Evenson, E. B., 2003a. Outburst flooding and surge initiation in response to climatic cooling: An hypothesis. Geomorphology. submitted.

Alley, R. B., Lawson, D., Evenson, E. B., Larson, G. and Baker, G., 2003b. Stabilizing feedbacks in glacier bed erosion. Nature, 424: 758–760.

Bachelor, G. K., 1967. An Introduction to Fluid Dynamics. Cambridge University Press, Cambridge, UK.

Becker, E. B., Carey, G. F. and Oden, J. T., 1981. Finite Elements: An Introduction. Prentice-Hall, Englewood Cliffs, N. J.

Bindschadler, R. and Vornberger, P., 1998. Changes in the West Antarctica ice sheet since 1963 from declassified satellite photography. Science, 279: 689–692.

Bond, G. C., Showers, W., Elliot, M., Evans, M., Lotti, R., Hajdas, I., Bonani, G. and Johnson, S., 1999. The North Atlantic's 1-2 kyr climate rhythm: relation to Heinrich events, Dansgaard/Oeschger cycles and the Little Ice Age. In: Clark, P. U., Webb, R. S. and Keigwin, L. D. (Editors), Mechanisms of Global Climate Change at Millennial Time Scales. Vol. 112 of Geophysical Monograph. American Geophysical Union, Washington D. C., pp. 35–58.

Broecker, W. S., 1994. Massive iceberg discharges as triggers for global climate change. Nature, 372: 421–424.

Budd, W. F., 1970. Ice flow over bedrock perturbations. Journal of Glaciology, 9: 29–48.

Cutler, P. M., Colgan, P. M. and Mickelson, D. M., 2002. Sedimentologic evidence for outburst floods from the Laurentide Ice Sheet margin in Wisconsin, USA: implications for tunnel-channel formation. Quaternary International, 90: 23–40.

Drewry, D. J. (Editor), 1983. Antarctica: Glaciological and Geophysical Folio. Scott Polar Research Institute, University of Cambridge, Cambridge, UK.

Hallet, B., Hunter, L. and Bogen, J., 1996. Rates of erosion and sediment evacuation by glaciers: A review of field data and their implications. Global and Planetary Change, 12: 213–235.

Hindmarsh, R. and Le Meur, E., 2001. Dynamical processes involved in the retreat of marine ice sheets. Journal of Glaciology, 47: 271–282.

Hindmarsh, R. and Le Meur, E., 2002. Dynamical processes involved in the retreat of marine ice sheets (47, pg 271, 2001). Journal of Glaciology, 48: 174.

Hoffman, P. F., Kaufman, A. J., Halverson, G. P. and Schrag, D. P., 1998. A Neoproterozoic snowball earth. Science, 281: 1343–1346.

Hooke, R. L., 1998. Principles of Glacier Mechanics. Prentice Hall, Upper Saddle River, N.J.

Houghton, J. T., Filho, L. G. M., Callander, B. A., Harris, N., Kattenberg, A. and Maskell, K. (Editors). 1995. Climate Change 1995: the Science of Climate Change. Cambridge University Press, New York.

Hughes, T. J., 1998. Ice Sheets. Oxford University Press, New York.

Hulbe, C. L., 1998. Heat Balance of West Antarctic Ice Streams, Investigated With a Numerical Model of Coupled Ice Sheet, Ice Stream, and Ice Shelf Flow. Ph.D. Thesis, University of Chicago.

Jacobs, S. S., Hellmer, H. H. and Jenkins, A., 1996. Antarctic ice sheet melting in the Southeast Pacific. Geophysical Research Letters, 23: 957–960.

Johannesson, T., 2002. Propagation of a subglacial flood wave during the initiation of a jokulhlaup. Hydrological Sciences Journal, 47: 417–434.

Joughin, I., Gray, L., Bindschadler, R., Price, S., Morse, D., Hulbe, C., Mattar, K. and Werner, C., 1999. Tributaries of West Antarctic ice streams revealed by RADARSAT interferometry. Science, 286: 283–286.

Kamb, B., 1964. Glacier geophysics. Science, 146: 353–365.

Le Meur, E. and Hindmarsh, R., 2001. Coupled marine-ice-sheet/earth dynamics using a dynamically consistent ice-sheet model and a self-gravitating viscous earth model. Journal of Glaciology, 47: 258–270.

MacAyeal, D. R., 1989. Large-scale ice flow over a viscous basal sediment: theory and application to Ice Stream B, Antarctica. Journal of Geophysical Research, 94: 4071–4087.

MacAyeal, D. R., 1992. Irregular oscillations of the West Antarctic ice sheet. Nature, 359: 29–32.

MacAyeal, D. R., 1997. Lessons in Ice-Sheet Modeling. revised edition.. unpublished.

MacAyeal, D. R. and Lange, M. A., 1988. Ice-shelf response to ice-stream discharge fluctuations II. Ideal rectangular ice shelf. Journal of Glaciology, 34: 128–135.

MacAyeal, D. R., Bindschadler, R. A., Shabtaie, S., Stephenson, S. and Bentley, C. R., 1987. Force, mass, and energy budgets of the Crary Ice Rise Complex, Antarctica. Journal of Glaciology, 33: 218–230.

MacAyeal, D. R., Bindschadler, R. A., Shabtaie, S., Stephenson, S. and Bentley, C. R., 1989. Correction to: Force, mass, and energy budgets of the Crary Ice Rise Complex, Antarctica. Journal of Glaciology, 35: 151–152.

Mercer, J. H., 1968. Antarctic ice and Sangamon sea level. In: IAHS publication No. 79. pp. 217–225.

Press, W. H., Teukolsky, S. A., Vetterling, W. T. and Flannery, B. P., 1992. Numerical Recipes in C. Cambridge University Press, New York, NY.

Rignot, E. J., 1998. Fast recession of a West Antarctic glacier. Science, 281: 549–551.

Rignot, E. J., Vaughan, D., Schmeltz, M., Dupont, T. and MacAyeal, D., 2002. Acceleration of Pine Island and Thwaites Glaciers, West Antarctica. Ann. Glaciol., 34: 189–194.

Scherer, R. P., Aldahan, A., Tulaczyk, S., Possnert, G., Engelhardt, H. and Kamb, B., 1998. Pleistocene collapse of the West Antarctic Ice Sheet. Science, 281: 82–85.

Schmeltz, M., Rignot, E., Dupont, T. K. and MacAyeal, D. R., 2002. Sensitivity of Pine Island Glacier, West Antarctica, to changes in ice-shelf and basal conditions: a model study. Journal of Glaciology, 48: 552–558.

Shepherd, A., Wingham, D. J., Mansley, J. A. D. and Corr, H. F. J., 2001. Inland thinning of Pine Island Glacier, West Antarctica. Science, 291: 862–864.

Shepherd, A., Wingham, D. J., Payne, T. and Skvarca, P., 2003. Larsen Ice Shelf has progressively thinned. Science, 302: 856–859.

Strang, G., 1986. Introduction to Applied Mathematics. Wellesley-Cambridge Press, Wellesly MA.

Studinger, M., Bell, R., Karner, G., Tikku, A., Holt, J., Richter, D. L. M. T. G., Kempf, S. D., Peters, M. E., Blankenship, D. D., Sweeney, R. E. and Rystrom, V. L., 2003. Ice cover, landscape setting, and geological framework of Lake Vostok, East Antarctica. Earth and Planetary Science Letters.

Swithinbank, C., 1986. Ice rises and ice rumples. Filchner-Ronne Ice Shelf Programme, Report 3. pp. 11-14, Alfred Wegener Institute for Polar and Marine Research, Bremerhaven.

Thomas, R. and MacAyeal, D. R., 1982. Derived characteristics of the Ross Ice Shelf. Journal of Glaciology, 28: 397–412.

Thomas, R. H. and Bentley, C. R., 1978. A model for Holocene retreat of the West Antarctic ice sheet. Quaternary Research, 10: 150–170.

Van der Veen, C. J., 1986. Ice Sheets, Atmosphereic CO_2 and Sea Level. Ph.D. Thesis, State University of Utrecht.

Van der Veen, C. J. and Whillans, I. M., 1996. Model experiments on the evolution and stability of ice streams. Journal of Glaciology, 23: 129–137.

Warrick, R. A., Provost, C. L., Meier, M. F., Oerlemans, J. and Woodworth, P. L., 1995. Changes in sea level. In: *Houghton et al.* [1995]. pp. 363–397.

Weertman, J., 1961. Stability of ice-age ice sheets. Journal of Geophysical Research, 66: 3783–3792.

Weertman, J., 1964. Glacier sliding. Journal of Glaciology, 5: 287–303.

Weertman, J., 1974. Stability of the junction of an ice sheet and an ice shelf. Journal of Glaciology, 13: 3–11.

Whillans, I. M. and Van der Veen, C. J., 1993. New and improved determinations of velocity of ice streams B and C, West Antarctica. Journal of Glaciology, 39: 483–490.

Whillans, I. M., Bentley, C. R. and Van der Veen, C. J., 2001. Ice streams B and C. In: Alley, R. B. and Bindschadler, R. A. (Editors), The West Antarctic Ice Sheet: Behavior and Environment. Vol. 77 of Antarctic Research Series. pp. 257–281. American Geophysical Union, Washington, D.C.

Vita

Professional Preparation

University of Maine (Orono), Geological Sciences, B.S., 1994

University of Maine (Orono), Quaternary Studies, M.S., 1996

Pennsylvania State University, Geosciences, Ph.D., 2004

Appointments

Research Assistant/Associate, Penn State University (present)

Graduate Teaching and Research Assistant, Penn State University (Fall 1996 - Fall 2003)

Participant, Siple Dome Ice Core Project, 1998-1999 Antarctic

Field Season Research Assistant, University of Maine (Fall 1994 – Spring 1996)

Publications

Alley, R. B., T. K. Dupont, B. R. Parizek, S. Anandakrishnan, D. E. Lawson, G. J. Larson, and E. B. Evenson, Outburst flooding and surge initiation in response to climatic cooling: An hypothesis, *Geomorphology*, in press.

Alley, R. B., S. Anandakrishnan, T. K. Dupont, and B. R. Parizek, Ice streams – fast, and faster?, *Comptes Rendus Physique*, submitted.

Rignot, E. J., D. G. Vaughan, M. Schmeltz, T. Dupont, and D. MacAyeal, Acceleration of Pine Island and Thwaites Glaciers, West Antarctica, *Annals of Glaciology*, *34*, 189–194, 2002.

Schmeltz, M., E. Rignot, T. K. Dupont, and D. R. MacAyeal, Sensitivity of Pine Island Glacier, West Antarctica, to changes in ice-shelf and basal conditions: a model study, *Journal of Glaciology*, *48*(163), 552–558, 2002.